Chapter 10

Propagation Through Complex Paraxial *ABCD* Optical Systems

Overview: The purpose of this chapter is to introduce the basic characteristics of a *Gaussian-beam wave* propagating through an optical system composed of one or more optical elements aligned on the optical axis between the input and output planes in the presence of atmospheric turbulence. This technique, which once again utilizes the paraxial approximation, is based on a scheme of representing optical elements by the 2×2 *ABCD* ray matrices that were introduced in Chap. 4 for free-space propagation. We consider cases in which atmospheric effects exist along the entire propagation path, or are confined to only a portion of the path between input and output planes.

Building off the development in Chap. 4 and its extension in Chap. 5 to include atmospheric effects, we specialize expressions for the second-order statistical moments $E_2(\mathbf{r}_1, \mathbf{r}_2)$ and $E_3(\mathbf{r}_1, \mathbf{r}_2)$ primarily for the case of a single optical element that we model as a "Gaussian lens," viz., a combination

of a thinlens and finite aperture stop known also as a "soft lens." Optical receiver systems which use a large collecting lens to focus the light onto a photodetector to reduce scintillation (i.e., to induce *aperture averaging*) represent one area of application where the *ABCD* technique has proven to be quite effective. In particular, we derive expressions for the irradiance flux variance in the plane of the photodetector for several cases of interest, including that of a Gaussian-beam wave. We take into account both inner scale and outer scale effects through use of the modified atmospheric spectrum and we use the method of Chap. 9 to extend results into the moderate-to-strong fluctuation regimes.

10.1 Introduction

Most of the methods used for line-of-sight propagation problems do not readily adapt to propagation systems involving one or more optical elements along the path. However, a technique involving a *generalized extended Huygens-Fresnel principle* has been developed by Yura and Hanson [1,2] for atmospheric paraxial wave propagation through any complex optical system characterized by an *ABCD* ray matrix. When adapted specifically for the weak fluctuation regime based on the *Rytov approximation*, the *ABCD* method greatly simplifies the analysis as compared with other techniques [3].

In Sections 4.8 and 4.9 we introduced the *ABCD* method of analysis for free-space propagation and developed the diffractive properties of a Gaussian-beam wave for propagation through various complex paraxial optical systems displaying rotational symmetry. We followed this in Section 5.6 with a general development of the Rytov approximation for such optical systems in the presence of a random medium along the propagation path. In this chapter we will adapt the Rytov approximation to certain optical systems involving a single optical element under weak and strong irradiance fluctuations, and then briefly extend the technique to an *ABCD* optical system with N elements.

10.2 Single Element Optical System

The use of *ABCD ray matrices* permits us to describe the propagation of a Gaussian beam through a train of optical elements by utilizing the cascade scheme of multiplying successive matrix representations of each optical element, including those that describe the free-space path between optical elements [4]. In this fashion the entire propagation path, consisting of various optical elements at arbitrary positions along the propagation path, can be represented by a single *ABCD* ray matrix. As in Chap. 4, this method is based on the *paraxial approximation*, which is valid when the separation distance between optical elements is large compared with the transverse extent of the beam.

Within the framework of weak-to-strong conditions of optical turbulence and *ABCD* ray-matrix representations, the extended form of the Rytov method (Chaps. 5 and 9) is further developed in this chapter for the analysis of Gaussian-beam wave propagation through a random medium and a single (perfectly aligned) rotationally symmetric optical element somewhere along the propagation path between the input and output planes. To begin, however, we will briefly review the various propagation parameters of an optical wave in *free space* as developed in Chap. 4.

10.2.1 Free-space propagation

Let us consider the special configuration in which a single "thin lens" with focal length F_G and limiting aperture stop of effective transmission radius W_G exists between the input plane (transmitter) and the output plane (photodetector) as illustrated in Fig. 10.1. Because of the way we model it, we call such an element a "Gaussian lens." Here we let L_1 denote the distance from the input plane to the Gaussian lens whereas L_2 denotes the distance from the lens to the output plane for a total propagation distance $L = L_1 + L_2$.

Given the configuration shown in Fig. 10.1, the overall *ABCD* matrix is

$$\begin{aligned}\begin{pmatrix} A & B \\ C & D \end{pmatrix} &= \begin{pmatrix} 1 & L_2 \\ 0 & 1 \end{pmatrix}\begin{pmatrix} 1 & 0 \\ i\alpha_G & 1 \end{pmatrix}\begin{pmatrix} 1 & L_1 \\ 0 & 1 \end{pmatrix} \\ &= \begin{pmatrix} 1 + i\alpha_G L_2 & L_1 + L_2(1 + i\alpha_G L_1) \\ i\alpha_G & 1 + i\alpha_G L_1 \end{pmatrix},\end{aligned} \tag{1}$$

where

$$\alpha_G = \frac{2}{kW_G^2} + i\frac{1}{F_G}. \tag{2}$$

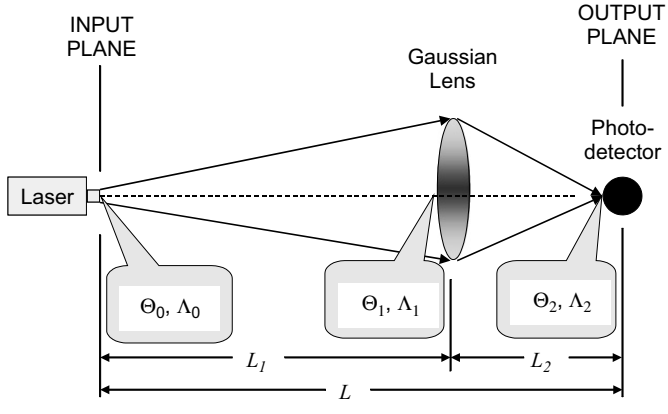

Figure 10.1 Propagation geometry for a Gaussian beam originating at distance L_1 to the left of a thin Gaussian lens of real focal length F_G and effective transmission radius W_G.

In the absence of atmospheric turbulence, the free-space field of a Gaussian-beam wave at the output plane in Fig. 10.1 is determined by the *generalized Huygens-Fresnel integral* [see Eq. (98) in Chap. 4]

$$U_0(\mathbf{r}, L) = -\frac{ik}{2\pi B}\exp(ikL)\int\int_{-\infty}^{\infty} d^2s \exp\left(-\frac{1}{2}\alpha_0 k s^2\right)\exp\left[\frac{ik}{2B}(As^2 - 2\mathbf{s}\cdot\mathbf{r} + Dr^2)\right]$$

$$= \frac{1}{p(L)}\exp(ikL)\exp\left[-\frac{1}{2}\alpha(L)kr^2\right], \tag{3}$$

where $A = A(L)$, $B = B(L)$, $C = C(L)$, and $D = D(L)$ are the ray-matrix elements in Eq. (1) and

$$\alpha_0 = \frac{2}{kW_0^2} + i\frac{1}{F_0}, \tag{4}$$

$$p(L) = A + i\alpha_0 B, \tag{5}$$

$$\alpha(L) = \frac{\alpha_0 D - iC}{A + i\alpha_0 B} = \frac{2}{kW^2} + i\frac{1}{F}. \tag{6}$$

To describe the beam characteristics at the input plane, the front plane of the Gaussian lens, and the plane of the photodetector, it is useful to introduce three sets of nondimensional beam parameters (see Section 4.9). To begin, we assume the transmitted Gaussian beam at the input plane has finite radius W_0 and phase front radius of curvature given by F_0. Thus, we have

$$z = 0: \qquad \Theta_0 = 1 - \frac{L_1}{F_0}, \quad \Lambda_0 = \frac{2L_1}{kW_0^2}, \tag{7}$$

$$z = \mathrm{L}_1: \qquad \Theta_1 = \frac{\Theta_0}{\Theta_0^2 + \Lambda_0^2} = 1 + \frac{L_1}{F_1},$$

$$\overline{\Theta}_1 = 1 - \Theta \tag{8}$$

$$\Lambda_1 = \frac{\Lambda_0}{\Theta_0^2 + \Lambda_0^2} = \frac{2L_1}{kW_1^2},$$

$$z = L_1 + L_2: \qquad \Theta_2 = \frac{L_1}{L_2}\left[\frac{L_1/L_2 - L_1/F_G + \overline{\Theta}_1}{(L_1/L_2 - L_1/F_G + \overline{\Theta}_1)^2 + (\Lambda_1 + \Omega_G)^2}\right] = 1 + \frac{L_2}{F},$$

$$\overline{\Theta}_2 = 1 - \Theta_2 \tag{9}$$

$$\Lambda_2 = \frac{L_1}{L_2}\left[\frac{\Lambda_1 + \Omega_G}{(L_1/L_2 - L_1/F_G + \overline{\Theta}_1)^2 + (\Lambda_1 + \Omega_G)^2}\right] = \frac{2L_2}{kW^2}.$$

In Eqs. (8), the parameters W_1 and F_1 denote the beam radius and phase front radius of curvature, respectively, in the front plane of the lens, and W and F in

Eqs. (9) are the same in the output plane (detector plane). Also, we have introduced the lens Fresnel parameter

$$\Omega_G = \frac{2L_1}{kW_G^2}. \tag{10}$$

10.2.2 Statistical moments

In the presence of optical turbulence along the entire propagation path, or some portion of it, the optical field at the output plane ($z = L = L_1 + L_2$) under the Rytov approximation is described by

$$U(\mathbf{r}, L) = U_0(\mathbf{r}, L) \exp\big[\psi_1(\mathbf{r}, L) + \psi_2(\mathbf{r}, L) + \cdots\big], \tag{11}$$

where $U_0(\mathbf{r}, L)$ is the unperturbed field defined by Eq. (3), and $\psi_1(\mathbf{r}, L)$ and $\psi_2(\mathbf{r}, L)$ represent first-order and second-order complex phase perturbations, respectively, caused by the random medium. To calculate the second-order and fourth-order moments of the random field (11), we will use a specialization of the *ABCD* spectral representation developed in Section 5.6 for the complex phase perturbation $\psi_1(\mathbf{r}, L)$. Doing so will enable us to generalize the statistical moments $E_2(\mathbf{r}_1, \mathbf{r}_2) = \langle \psi_1(\mathbf{r}_1, L)\psi_1^*(\mathbf{r}_2, L)\rangle$ and $E_3(\mathbf{r}_1, \mathbf{r}_2) = \langle \psi_1(\mathbf{r}_1, L)\psi_1(\mathbf{r}_2, L)\rangle$ defined, respectively, by Eqs. (22) and (23) in Chap. 6 for line-of-sight propagation. That is, these particular quantities take on somewhat different forms when one or more optical elements exist along the propagation path. Nonetheless, it can be shown that the quantity $E_1(0, 0) = \langle \psi_2(\mathbf{r}, L)\rangle + (1/2)\langle \psi_1^2(\mathbf{r}, L)\rangle$, which is also used in the Rytov approximation when calculating optical field moments, remains the same in the presence of an *ABCD* optical system as it appears in line-of-sight propagation. That is, the quantity $E_1(0, 0)$ represents the phase variance of the wave (under a geometrical optics approximation) between input and output planes and, as such, is independent of beam characteristics (e.g., see Section 8.5).

In developing expressions for $E_2(\mathbf{r}_1, \mathbf{r}_2)$ and $E_3(\mathbf{r}_1, \mathbf{r}_2)$, the first-order complex phase perturbation term $\psi_1(\mathbf{r}, L)$ must be expressed as a sum of integrals over the line-of-sight portions of the path connecting each optical element between input and output planes. For a single element optical system such as that shown in Fig. 10.1, the first-order complex phase perturbation can be expressed as [see Eq. (85) in Chap. 5]

$$\begin{aligned}
\psi_1(\mathbf{r}, L) &= ik \int_0^{L_1+L_2} \int\int_{-\infty}^{\infty} \exp\left[i\gamma \mathbf{K} \cdot \mathbf{r} - \frac{i\kappa^2 \gamma}{2k} B(z; L) \right] d\nu(\mathbf{K}, z)\, dz \\
&= ik \int_0^{L_1} \int\int_{-\infty}^{\infty} \exp\left[i\gamma_1 \mathbf{K} \cdot \mathbf{r} - \frac{i\kappa^2 \gamma_1}{2k} B(z; L) \right] d\nu(\mathbf{K}, z)\, dz \\
&\quad + ik \int_0^{L_2} \int\int_{-\infty}^{\infty} \exp\left[i\gamma_2 \mathbf{K} \cdot \mathbf{r} - \frac{i\kappa^2 \gamma_2}{2k} B(z'; L_2) \right] d\nu(\mathbf{K}, z')\, dz',
\end{aligned} \tag{12}$$

where γ_1 represents the path amplitude ratio between the input plane and the lens, γ_2 represents the path amplitude ratio between the lens and the output plane, and $z' = z - L_1$ in the last integral. Over the interval $0 \le z \le L_1$, the quantity $p(z) = A(z) + i\alpha_0 B(z)$ is based on the matrix elements

$$\begin{pmatrix} A(z) & B(z) \\ C(z) & D(z) \end{pmatrix} = \begin{pmatrix} 1 & z \\ 0 & 1 \end{pmatrix} = \begin{pmatrix} 1 & L_1(1-\xi) \\ 0 & 1 \end{pmatrix}, \qquad 0 \le z \le L_1, \tag{13}$$

where $\xi = 1 - z/L_1$. Consequently, we find

$$\gamma_1 = \frac{p(z)}{p(L_1 + L_2)} = (\Theta - i\Lambda)\xi + (\Theta_2 - i\Lambda_2)(1-\xi), \qquad 0 \le \xi \le 1, \tag{14}$$

where we recall that $\Theta \pm i\Lambda = (\Theta_1 \pm i\Lambda_1)(\Theta_2 \pm i\Lambda_2)$ [see Eq. (124) in Chap. 4]. Similarly, for $p(z) = A(z) + i\alpha_0 B(z)$ over the interval $L_1 \le z \le L_1 + L_2$ $(0 \le z' \le L_2)$, we find

$$\begin{aligned} \begin{pmatrix} A(z) & B(z) \\ C(z) & D(z) \end{pmatrix} &= \begin{pmatrix} 1 & z' \\ 0 & 1 \end{pmatrix} \begin{pmatrix} 1 & 0 \\ i\alpha_G & 1 \end{pmatrix} \begin{pmatrix} 1 & L_1 \\ 0 & 1 \end{pmatrix} \\ &= \begin{pmatrix} 1 + i\alpha_G L_2 \eta & L_1 + (1 + i\alpha_G L_1) L_2 \eta \\ i\alpha_G & 1 + i\alpha_G L_1 \end{pmatrix}, \qquad 0 \le z' \le L_2, \end{aligned} \tag{15}$$

where $\eta = z'/L_2$, and thus

$$\begin{aligned} \gamma_2 &= \frac{p(L_1 + z')}{p(L_1 + L_2)} \\ &= -(\Theta - i\Lambda) L_2 \eta / L_1 + (\Theta_2 - i\Lambda_2)(1 + L_2\eta/L_1 + i\alpha_G L_2 \eta), \qquad 0 \le \eta \le 1. \end{aligned} \tag{16}$$

The element $B(z; L)$, $0 \le z < L_1$ is the same as that of a reciprocal propagating beam from the output plane through the lens to position z (Section 5.6). Therefore,

$$B(z; L) \equiv B_1(\xi) = L_2 + (1 + i\alpha_G L_2) L_1 \xi, \qquad 0 \le \xi \le 1, \tag{17}$$

formally obtained from the B element in (15) with a reversal of the roles of L_1 and L_2. Similarly, the element between the lens and output plane is

$$B(z';\ L_2) \equiv B_2(\eta) = L_2(1 - \eta), \qquad 0 \le \eta \le 1. \tag{18}$$

If the random medium over each link is statistically independent of that over the other link (excluding double-passage waves) and the random medium is

statistically homogeneous and isotropic, the second-order moment $E_1(0,0)$ and the above results yield (on replacing η with ξ)

$$E_1(0,0) = -2\pi^2 k^2 L_1 \int_0^1 \int_0^\infty \kappa \Phi_n(\kappa)\, d\kappa\, d\xi - 2\pi^2 k^2 L_2 \int_0^1 \int_0^\infty \kappa \Phi_n(\kappa)\, d\kappa\, d\xi, \tag{19}$$

$$\begin{aligned} E_2(\mathbf{r}_1, \mathbf{r}_2) = {} & 4\pi^2 k^2 L_1 \int_0^1 \int_0^\infty \kappa \Phi_n(\kappa) J_0\big(\kappa|\gamma_1 \mathbf{r}_1 - \gamma_1^* \mathbf{r}_2|\big) \\ & \times \exp\left\{-\frac{i\kappa^2}{2k}\big[\gamma_1 B_1(\xi) - \gamma_1^* B_1^*(\xi)\big]\right\} d\kappa\, d\xi \\ & + 4\pi^2 k^2 L_2 \int_0^1 \int_0^\infty \kappa \Phi_n(\kappa) J_0\big(\kappa|\gamma_2 \mathbf{r}_1 - \gamma_2^* \mathbf{r}_2|\big) \\ & \times \exp\left\{-\frac{i\kappa^2}{2k}\big[\gamma_2 B_2(\xi) - \gamma_2^* B_2^*(\xi)\big]\right\} d\kappa\, d\xi, \end{aligned} \tag{20}$$

$$\begin{aligned} E_3(\mathbf{r}_1, \mathbf{r}_2) = {} & -4\pi^2 k^2 L_1 \int_0^1 \int_0^\infty \kappa \Phi_n(\kappa)\, J_0\big(\gamma_1 \kappa \rho\big) \exp\left[-\frac{i\kappa^2}{k} \gamma_1 B_1(\xi)\right] d\kappa\, d\xi \\ & - 4\pi^2 k^2 L_2 \int_0^1 \int_0^\infty \kappa \Phi_n(\kappa) J_0\big(\gamma_2 \kappa \rho\big) \exp\left[-\frac{i\kappa^2}{k} \gamma_2 B_2(\xi)\right] d\kappa\, d\xi, \end{aligned} \tag{21}$$

where $\kappa = |\mathbf{K}|$ and $\rho = |\mathbf{r}_1 - \mathbf{r}_2|$.

Equations (20) and (21) are more general than Eqs. (22) and (23) in Chap. 6, but reduce to those results for line-of-sight propagation (i.e., $\alpha_G = 0$). Observe, however, that if we assume the random medium exists only between the input plane and the lens (see Fig. 10.2), then those integrals in (19)–(21) with the subscript 2 are set to zero because $\Phi_n(\kappa) = 0$, $L_1 \le z \le L$. If we assume the random

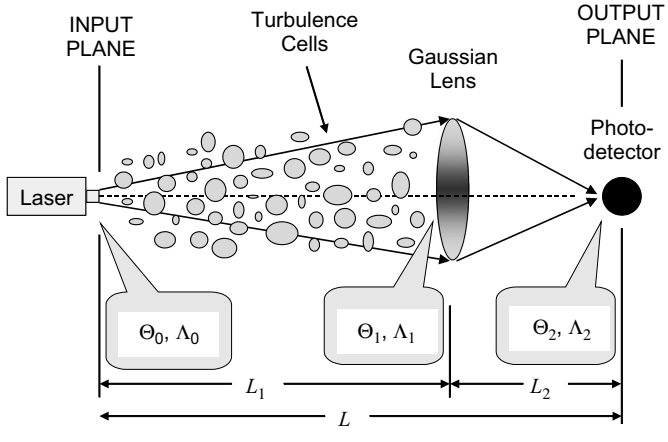

Figure 10.2 Same as Fig. 10.1 except for the presence of atmospheric turbulence between the input plane and the Gaussian lens.

medium exists only between the lens and the output plane, then the integrals with the subscript 1 are set to zero.

Some simplifications in the above results take place for the special case of a point source (spherical wave) at the emitting aperture ($\Theta_1 = \Lambda_1 = 0$). For example, we find that Eqs. (9) simplify to

$$\Theta_2 = \frac{L_1}{L_2}\left[\frac{L_1/L_2 - L_1/F_G + 1}{(L_1/L_2 - L_1/F_G + 1)^2 + \Omega_G^2}\right],$$
$$\Lambda_2 = \frac{L_1}{L_2}\left[\frac{\Omega_G}{(L_1/L_2 - L_1/F_G + 1)^2 + \Omega_G^2}\right]. \tag{22}$$

Also, the path amplitude ratios (14) and (16) reduce to

$$\gamma_1 = (\Theta_2 - i\Lambda_2)(1 - \xi),$$
$$\gamma_2 = (\Theta_2 - i\Lambda_2)(1 + L_2\xi/L_1 + i\alpha_G L_2 \xi). \tag{23}$$

10.2.3 Fourier-transform-plane analysis

One of the most remarkable properties of a converging lens is its inherent ability to perform a two-dimensional Fourier transform. That is, if a small object is placed in the front (or left-hand) focal plane of a "sufficiently large" thin converging lens, its Fourier transform will appear in the back (or right-hand) focal plane. With this in mind, let us consider the *Fourier-transform propagation geometry* in which the object and observation point are located in the front and back focal planes of a given lens (see Fig. 10.3). In this case $L_1 = L_2 = F_G$. If the object at the front focal plane is a collimated beam of radius W_0, then the beam described by (3) in the back focal plane of a large lens takes the form

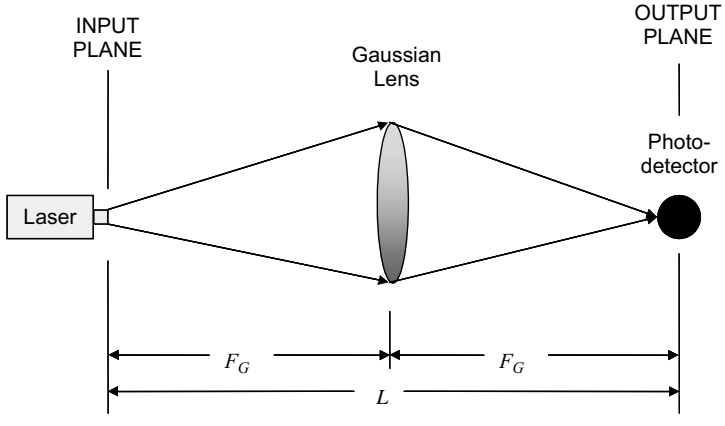

Figure 10.3 Propagation geometry for a Fourier-transform-plane analysis. We assume a thin Gaussian lens of real focal length F_G and effective transmission radius W_G.

$$U_0(\mathbf{r}, L) = U_0(\mathbf{r}, 2F_G) = -\frac{ikW_0^2}{2F_G}\exp(2ikF_G)\exp\left(-\frac{k^2W_0^2r^2}{4F_G^2}\right), \tag{24}$$

which, by defining $v = kr/F_{\mathrm{G}}$, is proportional to the Fourier transform of the input beam.

Let us now treat the special case in which a point source is in the front focal plane of a finite lens. Here, the overall *ABCD* matrix of Eq. (1) reduces to

$$\begin{pmatrix} A & B \\ C & D \end{pmatrix} = \begin{pmatrix} i\Omega_G & F_G(1+i\Omega_G) \\ -\dfrac{1}{F_G}(1+i\Omega_G) & i\Omega_G \end{pmatrix}, \tag{25}$$

where once again we set $\Omega_G = 2F_G/kW_G^2$. If the lens is sufficiently large so that $\Omega_G \ll 1$, then we can set $\Omega_G = 0$ in (25) to obtain the simpler (classic) result

$$\begin{pmatrix} A & B \\ C & D \end{pmatrix} = \begin{pmatrix} 0 & F_G \\ -\dfrac{1}{F_G} & 0 \end{pmatrix}. \tag{26}$$

From (14), (17), and (22), the relevant propagation and beam parameters for this particular configuration with $\Omega_G \neq 0$ are

$$\begin{aligned} \gamma_1 &= (\Theta_2 - i\Lambda_2)(1-\xi), \quad B_1(\xi) = F_G(1+i\xi\Omega_G), \\ \Theta_2 &= \frac{1}{1+\Omega_G^2}, \quad \Lambda_2 = \frac{\Omega_G}{1+\Omega_G^2}. \end{aligned} \tag{27}$$

The beam parameters in (27) indicate that the wave emerging from the lens behaves like a collimated beam with spot radius W_G.

Similar to that shown in Fig. 10.2, if we assume the random medium exists only between the point source and the lens, the second integral set with subscript 2 vanishes in each of Eqs. (19)–(21). Moreover, after some algebraic manipulation and change of dummy variable, we find that we can express Eqs. (20) and (21) as

$$\begin{aligned} E_2(\mathbf{r}_1, \mathbf{r}_2) = 4\pi^2k^2F_G \int_0^1 \int_0^\infty \kappa\Phi_n(\kappa) \\ \times J_0(|\Theta_2\mathbf{p} - 2i\Lambda_2\mathbf{r}|\kappa\xi)\exp\left(-\frac{\Lambda_2F_G\kappa^2\xi^2}{k}\right)d\kappa\, d\xi, \end{aligned} \tag{28}$$

$$\begin{aligned} E_3(\mathbf{r}_1, \mathbf{r}_2) = -4\pi^2k^2F_G \int_0^1 \int_0^\infty \kappa\Phi_n(\kappa)J_0[(\Theta_2 - i\Lambda_2)\kappa\xi\rho] \\ \times \exp\left(-\frac{\Lambda_2F_G\kappa^2\xi^2}{k}\right)\exp\left[-\frac{i\kappa^2F_G}{k}\xi(1-\overline{\Theta}_2\xi)\right]d\kappa\, d\xi, \end{aligned} \tag{29}$$

where $\mathbf{r} = (1/2)(\mathbf{r}_1 + \mathbf{r}_2)$, $\mathbf{p} = \mathbf{r}_1 - \mathbf{r}_2$, and $\rho = |\mathbf{p}|$. Based on the above representations, all statistical quantities developed in Chap. 6 for line-of-sight propagation

can likewise be developed for the Fourier-transform plane in the case of a point source at the transmitter. For example, the *mean irradiance* at the output plane is given by

$$\begin{aligned}\langle I(\mathbf{r}, 2F_G)\rangle &= I^0(\mathbf{r}, 2F_G)\exp[2E_1(0,0) + E_2(\mathbf{r},\mathbf{r})] \\ &= \frac{W_G^2}{W^2}\exp\left(-\frac{2r^2}{W^2}\right)\exp\left\{-4\pi^2 k^2 F_G \int_0^1\int_0^\infty \kappa\Phi_n(\kappa)\right. \\ &\quad \left.\times\left[1 - \exp\left(-\frac{\Lambda_2 F_G \kappa^2\xi^2}{k}\right)I_0(2\Lambda_2 r\kappa\xi)\right]d\kappa\, d\xi\right\},\end{aligned} \tag{30}$$

where $I^0(\mathbf{r}, 2F_G) = (W_G^2/W^2)\exp(-2r^2/W^2)$ is the irradiance in the absence of turbulence and $W = W_G\sqrt{(1+\Omega_G^2)}$ is the beam radius. Using the Kolmogorov power-law spectrum, Eq. (30) can be closely approximated by the Gaussian expression

$$\langle I(\mathbf{r}, 2F_G)\rangle \cong \frac{W_G^2}{W_{\mathrm{LT}}^2}\exp\left(-\frac{2r^2}{W_{\mathrm{LT}}^2}\right), \tag{31}$$

where the *long-term spot radius* of the Gaussian beam in this case is approximated by

$$\begin{aligned}W_{\mathrm{LT}} &= W\sqrt{1 + 1.33\sigma_R^2(F_G)\Lambda_2^{5/6}} \\ &= W_G\sqrt{1+\Omega_G^2}\sqrt{1 + 1.33\sigma_R^2(F_G)\Lambda_2^{5/6}},\end{aligned} \tag{32}$$

and $\sigma_R^2(F_G) = 1.23C_n^2 k^{7/6}F_G^{11/6}$.

Similarly, the *scintillation index* in the Fourier transform plane geometry is

$$\begin{aligned}\sigma_I^2(\mathbf{r}, 2F_G) &= 2\mathrm{Re}[E_2(\mathbf{r},\mathbf{r}) + E_3(\mathbf{r},\mathbf{r})] \\ &= 8\pi^2 k^2 F_G \int_0^1\int_0^\infty \kappa\Phi_n(\kappa)\exp\left(-\frac{\Lambda_2 F_G\kappa^2\xi^2}{k}\right) \\ &\quad\times\left\{I_0(2\Lambda_2 r\kappa\xi) - \cos\left[\frac{\kappa^2 F_G}{k}\xi(1-\overline{\Theta}_2\xi)\right]\right\}d\kappa\, d\xi.\end{aligned} \tag{33}$$

In the near field of the transform lens ($\Omega_G \ll 1$), Eq. (33) reduces to the scintillation index of an unbounded plane wave over a path of length F_G, whereas in the far field of the transform lens ($\Omega_G \gg 1$) Eq. (33) reduces to the scintillation index of a spherical wave. Between the near and far fields of the lens, the scintillation index (33) is mathematically equivalent to that associated with a collimated beam propagating backward from the lens over a path of length F_G. Hence,

under the assumption of a Kolmogorov spectrum, this quantity can be closely approximated by [3]

$$\sigma_I^2(\mathbf{r}, 2F_G) \cong 4.42\sigma_R^2(F_G)\left(\frac{\Omega_G}{1+\Omega_G^2}\right)^{5/6}\frac{r^2}{W^2} + 3.86\sigma_R^2(F_G)$$
$$\times\left\{\left(\frac{1+\Omega_G^2/9}{1+\Omega_G^2}\right)^{5/12}\cos\left[\frac{5}{6}\tan^{-1}\left(\frac{3+\Omega_G^2}{2\Omega_G}\right)\right] - \frac{11}{16}\left(\frac{\Omega_G}{1+\Omega_G^2}\right)^{5/6}\right\},$$
$$r \le W. \qquad (34)$$

The scintillation index (34), scaled by the spherical wave variance $\sigma_{I,\mathrm{sp}}^2(F_G) = 0.4\sigma_R^2(F_G)$, is shown in Fig. 10.4 (solid curves) for $r = 0$ and $r = W$, the latter case corresponding to the diffraction-limited edge of the beam.

If the transmitted wave at the front focal plane of the lens is a plane wave ($\Theta_1 = 1, \Lambda_1 = 0$), then $\Theta = \Theta_2 = 0$ and $\Lambda = \Lambda_2 = 1/\Omega_G$. In this case we find $\gamma_1 = -i/\Omega_G$, and, consequently,

$$E_2(\mathbf{r}_1, \mathbf{r}_2) = 4\pi^2 k^2 F_G \int_0^\infty \kappa\Phi_n(\kappa) I_0\left(\frac{2\kappa r}{\Omega_G}\right)\exp\left(-\frac{\kappa^2 F_G}{k\Omega_G}\right)d\kappa, \qquad (35)$$

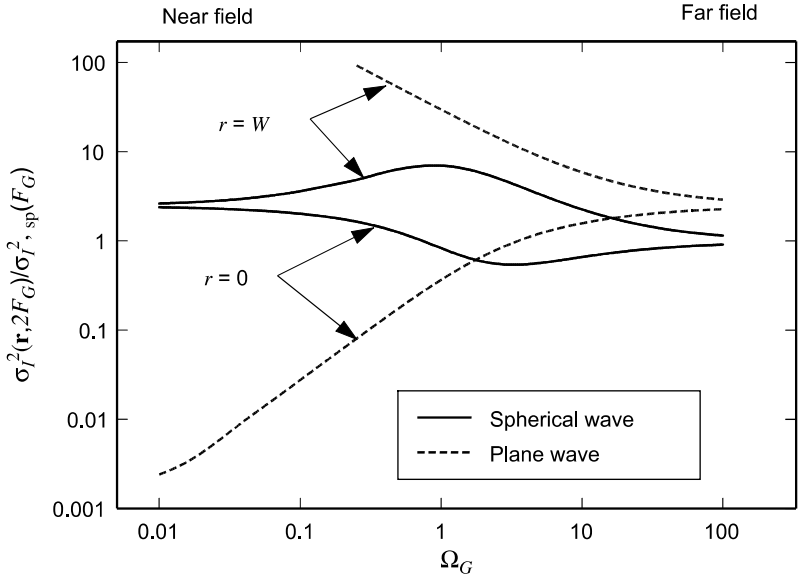

Figure 10.4 The normalized variance of irradiance (scaled by the spherical wave irradiance variance) as a function of Fresnel ratio $\Omega_G = 2F_G/kW_G^2$ for the Fourier-transform-plane propagation geometry.

$$E_3(\mathbf{r}_1,\mathbf{r}_2) = -4\pi^2 k^2 F_G \int_0^1 \int_0^\infty \kappa \Phi_n(\kappa) I_0\left(\frac{\kappa\rho}{\Omega_G}\right) \exp\left(-\frac{\kappa^2 F_G}{k\Omega_G}\right) \times \exp\left(-\frac{i\kappa^2 F_G \xi}{k}\right) d\kappa\, d\xi. \tag{36}$$

The *mean irradiance* for an incident plane wave becomes

$$\langle I(\mathbf{r}, 2F_G)\rangle = \frac{1}{\Omega_G^2} \exp(-2r^2/W^2) \exp\left\{-4\pi^2 k^2 F_G \int_0^\infty \kappa \Phi_n(\kappa) \times \left[1 - \exp\left(-\frac{\kappa^2 F_G}{k\Omega_G}\right) I_0(2\kappa r/\Omega_G)\right] d\kappa\right\}, \tag{37}$$

which, under the assumption of a Kolmogorov spectrum, can be approximated by

$$\langle I(\mathbf{r}, 2F_G)\rangle \cong \frac{1}{\Omega_G^2\left[1 + 3.54\sigma_R^2(F_G)\Omega_G^{-5/6}\right]} \exp\left\{-\frac{2r^2}{W^2\left[1 + 3.54\sigma_R^2(F_G)\Omega_G^{-5/6}\right]}\right\}, \tag{38}$$

where $W = 2F_G/kW_G$. The corresponding *scintillation index* takes the form

$$\sigma_I^2(\mathbf{r}, 2F_G) = 8\pi^2 k^2 F_G \int_0^1 \int_0^\infty \kappa \Phi_n(\kappa) \exp\left(-\frac{\kappa^2 F_G}{k\Omega_G}\right)\left[I_0\left(\frac{2\kappa r}{\Omega_G}\right) - \cos\left(\frac{\kappa^2 F_G \xi}{k}\right)\right] d\kappa\, d\xi, \tag{39}$$

or, assuming a Kolmogorov spectrum,

$$\sigma_I^2(\mathbf{r}, 2F_G) \cong 11.79\sigma_R^2(F_G)\Omega_G^{-5/6}\frac{r^2}{W^2} + 3.86\sigma_R^2(F_G) \times \left[\left(1 + \frac{1}{\Omega_G^2}\right)^{11/12} \sin\left(\frac{11}{6}\tan^{-1}\Omega_G\right) - \frac{11}{6}\Omega_G^{-5/6}\right], \qquad r \le W. \tag{40}$$

Equation (40), scaled by the spherical wave variance $\sigma_{I,\,\mathrm{sp}}^2(F_G) = 0.4\sigma_R^2(F_G)$, is shown in Fig. 10.4 (dashed curves) for $r = 0$ and $r = W$ (ignoring beam wander). Note that in the far field of the lens the scintillation index approaches that of a plane wave, whereas in the near field of the lens the scintillation index is similar to that of a focused beam.

10.2.4 Image-plane analysis

Another example of practical interest arises in imaging applications (see also Chap. 14). The analysis of this case in the absence of a random medium was presented in Section 4.10.2. Here we limit our analysis to the special case of a point source at the transmitter and assume the random medium exists only between the source and the lens (see Fig. 10.2). Thus, the relevant parameters are given by

$$\Theta_2 = 0, \quad \Lambda_2 = \frac{L_1}{L_2\Omega_G} = \frac{kW_G^2}{2L_2}, \tag{41}$$

$$\gamma_1 = -\frac{iL_1(1-\xi)}{L_2\Omega_G}, \quad B_1(\xi) = L_2(1-\xi+i\xi\Omega_G). \tag{42}$$

After some algebraic rearranging, we find that the moments (20) and (21) for this case reduce to

$$E_2(\mathbf{r}_1,\mathbf{r}_2) = 4\pi^2k^2L_1\int_0^1\int_0^\infty \kappa\Phi_n(\kappa)I_0\left(\frac{2\kappa\xi L_1 r}{L_2\Omega_G}\right)\exp\left(-\frac{L_1\kappa^2\xi^2}{k\Omega_G}\right)d\kappa\,d\xi, \tag{43}$$

$$E_3(\mathbf{r}_1,\mathbf{r}_2) = -4\pi^2k^2L_1\int_0^1\int_0^\infty \kappa\Phi_n(\kappa)I_0\left(\frac{\kappa\xi L_1\rho}{L_2\Omega_G}\right)$$
$$\times\exp\left(-\frac{L_1\kappa^2\xi^2}{k\Omega_G}\right)\exp\left[-\frac{iL_1\kappa^2}{k}\xi(1-\xi)\right]d\kappa\,d\xi. \tag{44}$$

The *Strehl ratio*, which is related to image resolution (Section 14.3), is considered one of the most important parameters of system performance for an optical imaging system. It is defined at the image plane of a receiver by the ratio of the on-axis mean irradiance in turbulence of a point source to that in the absence of turbulence. For a point source at the emitting aperture of the transmitter, the *mean irradiance* at the image plane of a thin lens can be expressed as

$$\langle I(\mathbf{r},L)\rangle = \frac{W_G^2}{W^2}\exp\left(-\frac{2r^2}{W^2}\right)\exp\left\{-4\pi^2k^2L_1\int_0^1\int_0^\infty \kappa\Phi_n(\kappa)\right.$$
$$\left.\times\left[1-\exp\left(-\frac{L_1\kappa^2\xi^2}{k\Omega_G}\right)I_0\left(\frac{2\kappa\xi L_1 r}{L_2\Omega_G}\right)\right]d\kappa\,d\xi\right\}, \tag{45}$$

where $L = L_1 + L_2$ and $W = 2L_2/kW_G$. Under the assumption of a Kolmogorov spectrum, the mean irradiance (45) can be approximated by the Gaussian form

$$\langle I(\mathbf{r},L)\rangle \cong \frac{W_G^2}{W^2\left[1+1.33\sigma_R^2(L_1)\Omega_G^{-5/6}\right]}\exp\left\{-\frac{2r^2}{W^2\left[1+1.33\sigma_R^2(L_1)\Omega_G^{-5/6}\right]}\right\}. \tag{46}$$

Hence, the Strehl ratio (SR) deduced from Eq. (46) is

$$\mathrm{SR} = \frac{\langle I(0,L)\rangle}{I^0(0,L)} \cong \frac{1}{1 + 1.33\sigma_R^2(L_1)\Omega_G^{-5/6}}. \tag{47}$$

It is customary to express the Strehl ratio as a function of telescope diameter D_G over atmospheric coherence length r_0. From the relationship $D_G^2 = 8W_G^2$ connecting the hard aperture diameter D_G with the Gaussian radius W_G, and $r_0 = (0.16C_n^2k^2L_1)^{-3/5}$ for a point source, the Strehl ratio (47) becomes

$$\mathrm{SR} \cong \frac{1}{1 + (D_G/r_0)^{5/3}}, \qquad D_G/r_0 < 1. \tag{48}$$

To compare Eq. (48) with results not limited to weak irradiance fluctuations, we note that the Strehl ratio under general conditions is defined by the integral [6]

$$\mathrm{SR} = \frac{16}{\pi}\int_0^1 u\left[\cos^{-1} u - u(1-u^2)^{1/2}\right]\exp\left[-3.44(uD_G/r_0)^{5/3}\right]du, \tag{49}$$

which can be closely approximated by the expression

$$\mathrm{SR} \cong \frac{1}{[1 + (D_G/r_0)^{5/3}]^{6/5}}. \tag{50}$$

The Strehl ratio as predicted by relations (49) and (50), which are theoretically valid under all conditions of atmospheric turbulence, is plotted in Fig. 10.5 as a function of D_G/r_0 along with that predicted by (48) (dashed curve). We can see that for sufficiently small telescope diameters in which $0 \le D_G/r_0 < 1$, (48) and (49)

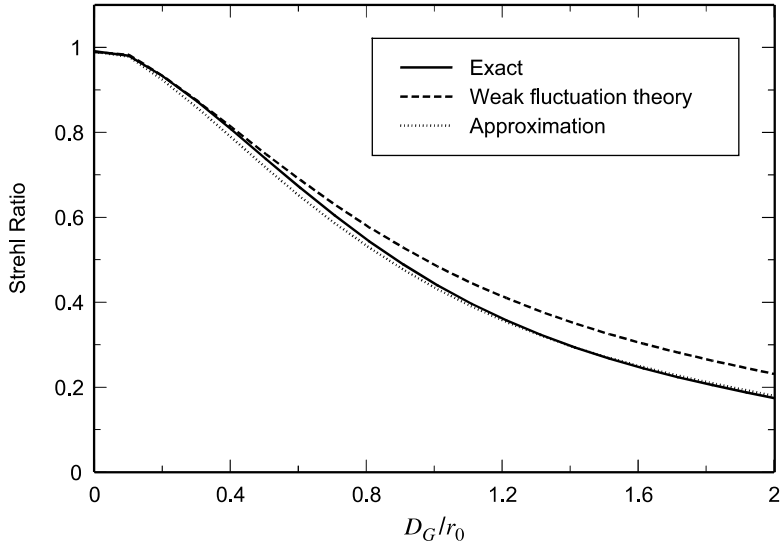

Figure 10.5 The Strehl ratio plotted as a function of D_G/r_0. The solid curve comes from Eq. (49), the dashed curve from (48), and the dotted curve from (50).

are in good agreement, whereas (50) provides an excellent approximation to (49) over all ranges.

For a point source at the transmitter, the longitudinal component of the *scintillation index* in the image plane is given by

$$\sigma_I^2(0,L) = 8\pi^2 k^2 L_1 \int_0^1 \int_0^\infty \kappa \Phi_n(\kappa) \exp\left(-\frac{L_1 \kappa^2 \xi^2}{k\Omega_G}\right) \times \left\{1 - \cos\left[\frac{L_1 \kappa^2}{k}\xi(1-\xi)\right]\right\} d\kappa\, d\xi, \tag{51}$$

which, based on the Kolmogorov spectrum, can be approximated for $\Omega_G > 1$ by

$$\sigma_I^2(0,L) = 3.86\sigma_R^2(L_1) \times \left\{0.4\left(1+\frac{4}{\Omega_G^2}\right)^{5/12} \cos\left[\frac{5}{6}\tan^{-1}(0.5\Omega_G)\right] - \frac{11}{16}\Omega_G^{-5/6}\right\}, \quad \Omega_G > 1. \tag{52}$$

When the point source is in the far field of the lens the variance (51) reduces to that of a spherical wave propagating over path length L_1, and in the near field of the lens, it acts like that of a large-aperture focused beam. Thus, the on-axis variance approaches $\sigma_I^2(0,L) \cong 2\sigma_R^2 \Omega_G^{7/6}, \Omega_G \ll 1$, where $\Omega_G^{7/6}$ is basically an aperture-averaging factor [2]. That is, for far-field conditions the lens lies within one correlation patch $\sqrt{L/k}$ of the incident irradiance, whereas many independent correlation patches exist in the near-field condition. In particular, the exact solution of (51), scaled by $\sigma_{I,\mathrm{sp}}^2 = 0.4\sigma_R^2$, can be interpreted as a spherical wave *aperture-averaging factor* (see also Section 10.3.3)

$$A = 9.66\,\mathrm{Re}\left[i^{5/6}{}_2F_1\left(-\frac{5}{6}, \frac{11}{6}; \frac{17}{6}; 1+\frac{ikD_G^2}{16L_1}\right) - \frac{11}{16}\left(\frac{kD_G^2}{16L_1}\right)^{5/6}\right], \tag{53}$$

where the Kolmogorov spectrum has been used.

10.3 Aperture Averaging

If the receiving aperture in an optical communication system is smaller than the correlation width of the irradiance fluctuations, then the aperture behaves essentially like a "point aperture." However, as the aperture size increases beyond the irradiance correlation width, the receiver "sees" several correlation patches and the scintillation level measured by the detector in the image plane begins to decrease. This effect, known as *aperture averaging*, is intentionally used in direct detection systems to reduce scintillation and, consequently, increase the mean signal-to-noise ratio (see Chap. 11).

The decrease in scintillation associated with increasing telescope collecting area had been recognized in early astronomical measurements made in the 1950s [7].

These same measurements revealed that scintillation reduction through aperture averaging causes a shift of the relative frequency content of the irradiance power spectrum toward lower frequencies—in essence, averaging out the fastest fluctuations. More recently, aperture averaging effects have been studied in the context of laser beam propagation through atmospheric turbulence [8–15].

The reduction in scintillation due to aperture averaging can be deduced from the ratio of power fluctuations by a finite-size collecting aperture to that obtained by a very small (point) aperture. The normalized variance of the power fluctuations in the receiver plane is the same as the *flux variance of irradiance fluctuations* defined by

$$\sigma_I^2(D_G) = \frac{\langle P^2\rangle - \langle P\rangle^2}{\langle P\rangle^2}$$

$$= \frac{16}{\pi D_G^2}\int_0^{D_G} \rho B_I(\rho, L)\left[\cos^{-1}\left(\frac{\rho}{D_G}\right) - \frac{\rho}{D_G}\sqrt{1-\frac{\rho^2}{D_G^2}}\right]d\rho, \qquad (54)$$

where P is the received optical power, D_G is the (hard) aperture diameter of a circular aperture, $B_I(\rho, L)$ is the irradiance covariance function in the pupil plane, and the terms in brackets arise from the *modulation transfer function* (MTF) of the circular aperture (see Section 14.3). The change of variable $x = \rho/D_G$ permits us to rewrite Eq. (54) as

$$\sigma_I^2(D_G) = \frac{16}{\pi}\int_0^1 xB_I(xD_G, L)\left(\cos^{-1}x - x\sqrt{1-x^2}\right)dx. \qquad (55)$$

The *aperture averaging factor* (or *coefficient*) A for a circular aperture of diameter D_G is defined by the ratio $A = \sigma_I^2(D_G)/\sigma_I^2(0)$, where $\sigma_I^2(0) = B_I(0, L)$ is the scintillation index for a point aperture ($D_G = 0$). In this case we write

$$A = \frac{\sigma_I^2(D_G)}{\sigma_I^2(0)} = \frac{16}{\pi}\int_0^1 xb_I(xD_G, L)\left(\cos^{-1}x - x\sqrt{1-x^2}\right)dx, \qquad (56)$$

where $b_I(\rho, L) = B_I(\rho, L)/B_I(0, L)$ is the *normalized* covariance function.

10.3.1 *ABCD* matrix formulation

Fried [9] used numerical integration to solve (56) for a plane wave. Exact analytic solutions along with tractable interpolation formulas were later developed by Andrews [13] for the Kolmogorov spectrum. However, both of these analyses were limited to weak fluctuation theory.

Here, we will not restrict our analysis to only weak fluctuation theory nor will we rely directly on Eq. (55) for the irradiance flux variance. Instead, we will calculate the irradiance flux variance under general irradiance fluctuation conditions on the optical axis in the plane of the photodetector behind the receiver collecting lens. To do so, we use the *ABCD* matrix formulation for an optical system

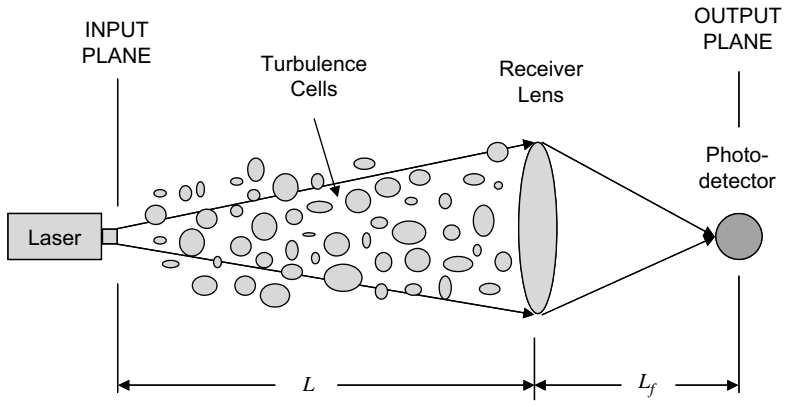

Figure 10.6 Propagation geometry for a Gaussian beam originating at distance L to the left of a thin Gaussian lens of real focal length F_G and effective transmission radius W_G.

consisting of a thin lens of focal length F_G and Gaussian limiting aperture of radius W_G. We illustrate such a system below in Fig. 10.6 where once again we assume that atmospheric turbulence exists only along the propagation path from the transmitter to the receiver lens, but here we will take a propagation path of length L. The beam is then focused onto the photodetector at a short distance L_f behind the lens. Pointing errors are neglected in this analysis.

Based on Eqs. (20) and (21) for weak irradiance fluctuations, the on-axis irradiance flux variance of a Gaussian-beam wave in the plane of the photodetector is given by

$$\begin{aligned}\sigma_I^2(D_G) &= 2\mathrm{Re}[E_2(0,0) + E_3(0,0)] \\ &= 8\pi^2 k^2 L \mathrm{Re} \int_0^1 \int_0^\infty \kappa \Phi_n(\kappa) \\ &\quad \times \left[\left[\exp\left\{ -\frac{i\kappa^2}{2k}\left[\gamma_1 B_1(\xi) - \gamma_1^* B_1^*(\xi)\right]\right\} - \exp\left[-\frac{i\kappa^2}{k}\gamma_1 B_1(\xi)\right]\right]\right] d\kappa\, d\xi,\end{aligned} \tag{57}$$

where the "hard aperture" diameter D_G of the receiver is related to the "soft aperture" radius W_G by $D_G^2 = 8W_G^2$. For a beam focused onto the photodetector in this plane, we set $L/L_f - L/F_G + \overline{\Theta}_1 = 0$, and hence, γ_1 and $B_1(\xi)$ reduce to [see (14) and (17)]

$$\begin{aligned}\gamma_1 &= -\frac{L}{L_f(\Lambda_1 + \Omega_G)}\left[\Lambda_1 \xi + i(1 - \overline{\Theta}_1 \xi)\right], \\ B_1(\xi) &= L_f(1 - \overline{\Theta}_1 \xi + i\Omega_G \xi).\end{aligned} \tag{58}$$

10.3.2 Plane wave

If the wave incident on the lens is a plane wave ($\Theta_1 = 1, \Lambda = 0$), then Eq. (57) becomes

$$\sigma_{I,\mathrm{pl}}^2(D_G) = 8\pi^2 k^2 L \int_0^1 \int_0^\infty \kappa \Phi_n(\kappa) \exp\left(-\frac{D_G^2 \kappa^2}{16}\right)\left(1 - \cos\frac{L\kappa^2 \xi}{k}\right) d\kappa \, d\xi. \quad (59)$$

Based on a conventional Kolmogorov power-law spectrum, this expression reduces to

$$\sigma_{I,\mathrm{pl}}^2(D_G) = 3.86\sigma_R^2 \left\{\left[1 + \left(\frac{kD_G^2}{16L}\right)^2\right]^{11/12} \sin\left[\frac{11}{6}\tan^{-1}\left(\frac{16L}{kD_G^2}\right)\right] - \frac{11}{6}\left(\frac{kD_G^2}{16L}\right)^{5/6}\right\}, \quad (60)$$

where $\sigma_R^2 = 1.23 C_n^2 k^{7/6} L^{11/6}$. A simple approximation for the aperture averaging factor from (60) under weak irradiance fluctuations (with $< 7\%$ error) is given by [13]

$$A = \left[1 + 1.062\left(\frac{kD_G^2}{4L}\right)\right]^{-7/6}, \qquad \sigma_R^2 < 1. \quad (61)$$

Under *general irradiance fluctuation conditions*, we use the large-scale filter function with both inner scale and outer scale parameters given by Eq. (50) in Chap. 9, which leads to (after a lengthy calculation) [15,16])

$$\sigma_{I,\mathrm{pl}}^2(D_G) = \exp\left[\sigma_{\ln X}^2(D_G, l_0) - \sigma_{\ln X}^2(D_G, L_0) + \frac{0.51\sigma_{PL}^2(1 + 0.69\sigma_{PL}^{12/5})^{-5/6}}{1 + 0.90d^2(\sigma_R/\sigma_{PL})^{12/5} + 0.62d^2\sigma_R^{12/5}}\right] - 1, \quad 0 \le \sigma_R^2 < \infty, \quad (62)$$

where

$$\sigma_{\ln X}^2(D_G, l_0) = 0.16\sigma_R^2\left(\frac{\eta_{Xd} Q_l}{\eta_{Xd} + Q_l}\right)^{7/6} \times \left[1 + 1.75\left(\frac{\eta_{Xd}}{\eta_{Xd} + Q_l}\right)^{1/2} - 0.25\left(\frac{\eta_{Xd}}{\eta_{Xd} + Q_l}\right)^{7/12}\right], \quad (63)$$

$$\sigma_{\ln X}^2(D_G, L_0) = 0.16\sigma_R^2\left(\frac{\eta_{Xd0} Q_l}{\eta_{Xd0} + Q_l}\right)^{7/6} \times \left[1 + 1.75\left(\frac{\eta_{Xd0}}{\eta_{Xd0} + Q_l}\right)^{1/2} - 0.25\left(\frac{\eta_{Xd0}}{\eta_{Xd0} + Q_l}\right)^{7/12}\right], \quad (64)$$

$$\eta_X = \frac{2.61}{1 + 0.45\sigma_R^2 Q_l^{1/6}}, \tag{65}$$

$$\eta_{Xd} = \frac{\eta_X}{1 + d^2\eta_X/4} = \frac{2.61}{1 + 0.65d^2 + 0.45\sigma_R^2 Q_l^{1/6}}, \tag{66}$$

$$\eta_{Xd0} = \frac{\eta_{Xd} Q_0}{\eta_{Xd} + Q_0} = \frac{2.61 Q_0}{2.61 + Q_0 + 0.65d^2 Q_0 + 0.45\sigma_R^2 Q_0 Q_l^{1/6}}, \tag{67}$$

$$d = \sqrt{\frac{kD_G^2}{4L}}, \quad Q_l = \frac{10.89L}{kl_0^2}, \quad Q_0 = \frac{64\pi^2 L}{kL_0^2}. \tag{68}$$

Also, the weak-fluctuation scintillation index σ_{PL}^2 based on the modified atmospheric spectrum [see Eq. (22) in Chap. 3] is defined by Eq. (48) in Chap. 9.

In the absence of inner scale and outer scale effects ($Q_l \to \infty$ and $Q_0 \to 0$), the irradiance flux variance (62) reduces to the simpler expression

$$\sigma_{I,\,\mathrm{pl}}^2(D_G) = \exp\left[\frac{0.49\sigma_R^2}{\left(1 + 0.65d^2 + 1.11\sigma_R^{12/5}\right)^{7/6}} + \frac{0.51\sigma_R^2\left(1 + 0.69\sigma_R^{12/5}\right)^{-5/6}}{1 + 0.90d^2 + 0.62d^2\sigma_R^{12/5}}\right] - 1. \tag{69}$$

In Fig. 10.7 we show the aperture averaging factor deduced from (69) as a function of circular aperture radius $D_G/2$ scaled by the Fresnel zone $\sqrt{L/k}$ under various values of the Rytov variance. In weak conditions the correlation scale of the irradiance fluctuations is defined by the size of the Fresnel zone; thus, significant aperture averaging takes place only when $D_G > 2\sqrt{L/k}$. The case $\sigma_R^2 = 4$ leads to a scintillation index of $\sigma_I^2(0) = 1.17$ in the pupil plane, which corresponds to a moderate fluctuation level approaching the focusing regime. In this regime the spatial coherence radius is equal to or smaller than the Fresnel zone. The last case $\sigma_R^2 = 50$ corresponds to the saturation regime in which the scintillation index is once again $\sigma_I^2(0) = 1.17$. The two-scale behavior in the aperture averaging factor in the saturation regime is determined first by the spatial coherence scale ρ_0, after which there is a leveling effect followed by a secondary roll-off related to the scattering disk $L/k\rho_0$ that predicts less aperture averaging than would occur under weaker fluctuation conditions.

In Fig. 10.8 we plot curves from (62) corresponding to aperture diameters of 1 mm and 10 mm with inner scale $l_0 = 3$ mm and outer scale $L_0 = 1$ m. In addition, we have also plotted the corresponding curves with infinite outer scale. Analogous to the case of a point aperture, the presence of a finite outer scale reduces the scintillation value of the received wave even when using a large receiver collecting lens.

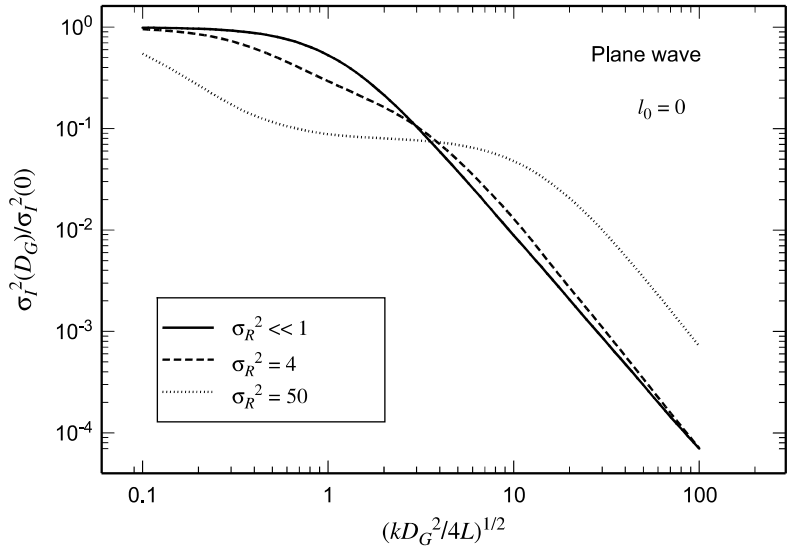

Figure 10.7 Aperture averaging factor for a plane wave under various irradiance fluctuation conditions.

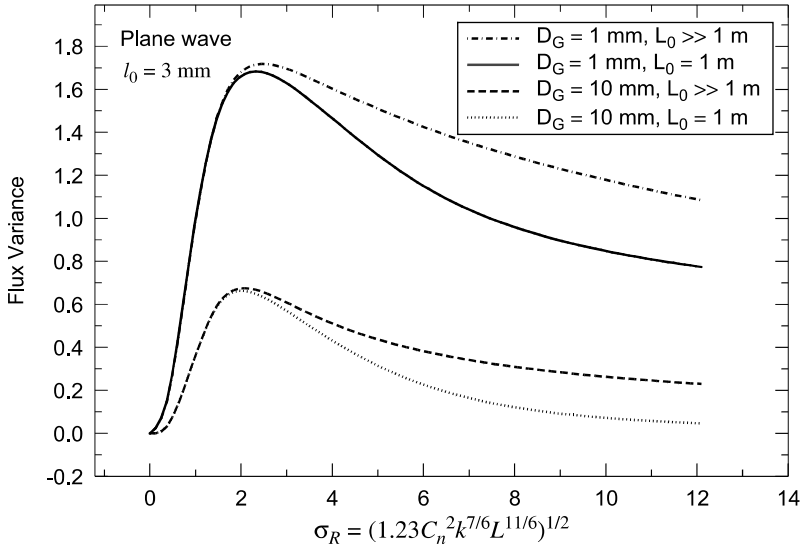

Figure 10.8 Irradiance flux variance of a plane wave vs. strength of turbulence and various aperture diameters. The assumed wavelength, inner scale, and refractive-index structure constant are, respectively, $\lambda = 0.633$ μm, $l_0 = 3$ mm, and $C_n^2 = 5 \times 10^{-13}$ m$^{-2/3}$.

10.3.3 Spherical wave

The irradiance flux variance (57) in the case of a spherical wave ($\Theta = \Lambda = 0$) and weak irradiance fluctuations takes the form

$$\sigma_{I,\,\mathrm{sp}}^2(D_G) = 8\pi^2 k^2 L \int_0^1 \int_0^\infty \kappa \Phi_n(\kappa) \exp\left(-\frac{D_G^2 \kappa^2 \xi^2}{16}\right) \times \left\{1 - \cos\left[\frac{L\kappa^2}{k}\xi(1-\xi)\right]\right\} d\kappa\, d\xi. \tag{70}$$

The aperture averaging factor deduced from (70) with a Kolmogorov spectrum is Eq. (53). However, by use of the strong fluctuation theory introduced in Chap. 9, it can be shown that the irradiance flux variance under general irradiance fluctuations is [15,16]

$$\sigma_{I,\,\mathrm{sp}}^2(D_G, l_0) = \exp\left[\sigma_{\ln X}^2(D_G, l_0) - \sigma_{\ln X}^2(D_G, L_0) + \frac{0.51\sigma_{SP}^2\left(1 + 0.69\sigma_{SP}^{12/5}\right)^{-5/6}}{1 + 0.90d^2\left(\beta_0/\sigma_{SP}\right)^{12/5} + 0.62d^2\beta_0^{12/5}}\right] - 1, \tag{71}$$

where $\beta_0^2 = 0.5C_n^2 k^{7/6} L^{11/6}$ and σ_{SP}^2 is the spherical wave scintillation index given by Eq. (75) in Chap. 9. Also,

$$\sigma_{\ln X}^2(D_G, l_0) = 0.04\beta_0^2 \left(\frac{\eta_{Xd} Q_l}{\eta_{Xd} + Q_l}\right)^{7/6} \times \left[1 + 1.75\left(\frac{\eta_{Xd}}{\eta_{Xd} + Q_l}\right)^{1/2} - 0.25\left(\frac{\eta_{Xd}}{\eta_{Xd} + Q_l}\right)^{7/12}\right], \tag{72}$$

$$\sigma_{\ln X}^2(D_G, L_0) = 0.04\beta_0^2 \left(\frac{\eta_{Xd0} Q_l}{\eta_{Xd0} + Q_l}\right)^{7/6} \times \left[1 + 1.75\left(\frac{\eta_{Xd0}}{\eta_{Xd0} + Q_l}\right)^{1/2} - 0.25\left(\frac{\eta_{Xd0}}{\eta_{Xd0} + Q_l}\right)^{7/12}\right], \tag{73}$$

$$\eta_X = \frac{8.56}{1 + 0.20\beta_0^2 Q_l^{1/6}}, \tag{74}$$

$$\eta_{Xd} = \frac{\eta_X}{1 + 0.02d^2\eta_X} = \frac{8.56}{1 + 0.18d^2 + 0.20\beta_0^2 Q_l^{1/6}}, \tag{75}$$

$$\eta_{Xd0} = \frac{\eta_{Xd} Q_0}{\eta_{Xd} + Q_0} = \frac{8.56 Q_0}{8.56 + Q_0 + 0.18d^2 Q_0 + 0.20\beta_0^2 Q_0 Q_l^{1/6}}. \tag{76}$$

If we allow the inner scale to vanish and the outer scale to be unbounded, the resulting irradiance flux variance (71) takes the simpler form

$$\sigma_{I,\,\mathrm{sp}}^2(D_G) = \exp\left[\frac{0.49\beta_0^2}{\left(1+0.18d^2+0.56\beta_0^{12/5}\right)^{7/6}} + \frac{0.51\beta_0^2\left(1+0.69\beta_0^{12/5}\right)^{-5/6}}{1+0.90d^2+0.62d^2\beta_0^{12/5}}\right] - 1. \tag{77}$$

We plot the aperture averaging factor deduced from (77) in Fig. 10.9 for several values of the Rytov variance β_0^2. Behavior shown here for the spherical wave is similar to that in Fig. 10.7 for a plane wave. When inner scale and outer scale effects are accounted for, the general behavior is also similar to the plane wave case depicted in Fig. 10.8.

10.3.4 Comparison with experimental data

Churnside [12] reported on experimental data from a series of measurements made on a spherical wave with $\lambda = 0.633\ \mu\mathrm{m}$ propagating in the weak fluctuation regime, two sets of which are shown in Fig. 10.10. The filled circles correspond to measurements made over a path of length 100 m at a height of 1.5 m. The atmospheric conditions were $C_n^2 = 5.19 \pm 1.54 \times 10^{-14}\ \mathrm{m}^{-2/3}$, $l_0 = 6.26 \pm 0.38$ mm, and the Fresnel zone size was $\sqrt{L/k} = 3.17$ mm. Thus, $Q_l = 2.48$ and $Q_0 = 0$,

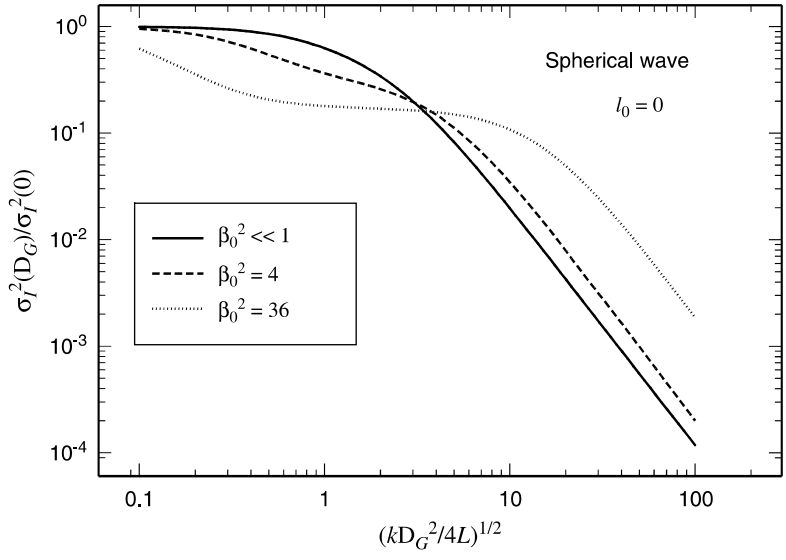

Figure 10.9 Aperture averaging factor associated with a spherical wave under various fluctuation conditions vs. aperture radius scaled by the Fresnel zone.

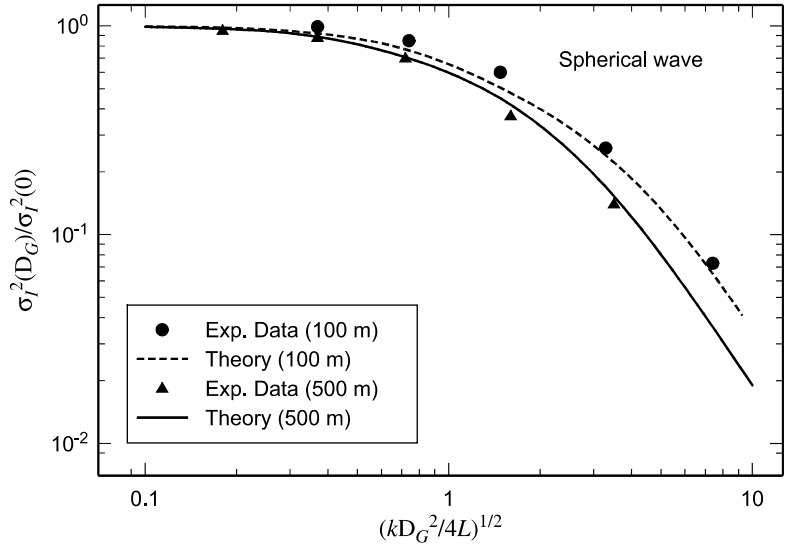

Figure 10.10 The filled circles and triangles correspond to experimental data from a spherical wave taken over paths of length 100 and 500 m, respectively, under weak fluctuation conditions [12]. The solid and dashed curves are from Eq. (71).

giving the dashed curve in Fig. 10.10 based on Eq. (71). The filled triangles correspond to measurements made over a path of length 500 m with $C_n^2 = 1.46 \pm 1.18 \times 10^{-13}\,\mathrm{m}^{-2/3}$, $l_0 = 7.19 \pm 0.90$ mm, and $\sqrt{L/k} = 7.10$ mm. Here, $Q_l = 13.88$ and $Q_0 = 0$, depicted by the solid curve in Fig. 10.10. The agreement between experimental data and the expression (71) is good in both cases, yielding a maximum error of roughly 15%.

Figures 10.11 and 10.12 show theoretical curves and experimental data [12] for two experiments over a 1000-m path. In Fig. 10.11, measured atmospheric parameters are $C_n^2 = 4.20 \pm 0.33 \times 10^{-13}\,\mathrm{m}^{-2/3}$ and $l_0 = 5.98 \pm 0.35$ mm, and in Fig. 10.12 the corresponding values are $C_n^2 = 1.29 \pm 0.39 \times 10^{-12}\,\mathrm{m}^{-2/3}$ and $l_0 = 7.57 \pm 0.55$ mm. Measured values of the scintillation index in the pupil plane, based on a 1-mm collecting aperture, are $\sigma_I^2(0) = 3.15 \pm 0.24$ and $\sigma_I^2(0) = 3.08 \pm 0.38$, respectively. According to our theoretical results, a collecting lens of 1 mm under these conditions will not act quite like a point aperture, but will exhibit a small amount of aperture averaging. Moreover, optical turbulence over the 1000 m range where the experiments were conducted is sufficiently strong that the outer scale can likely have an additional effect on the measured scintillation. The quantity ρ_0 appearing along the horizontal axis in each figure represents the spatial coherence radius of the received optical wave.

The dashed lines shown in Figs. 10.11 and 10.12 represent the theoretical model developed by Churnside [12]. During the experiment the height of the transmitter and receiver was reported to be approximately 1.5 m above ground. To closely match the calculated scintillation index with measured values for a 1-mm receiver aperture, in Fig. 10.11 we use an outer-scale value of $L_0 = 0.25$ m, which yields a

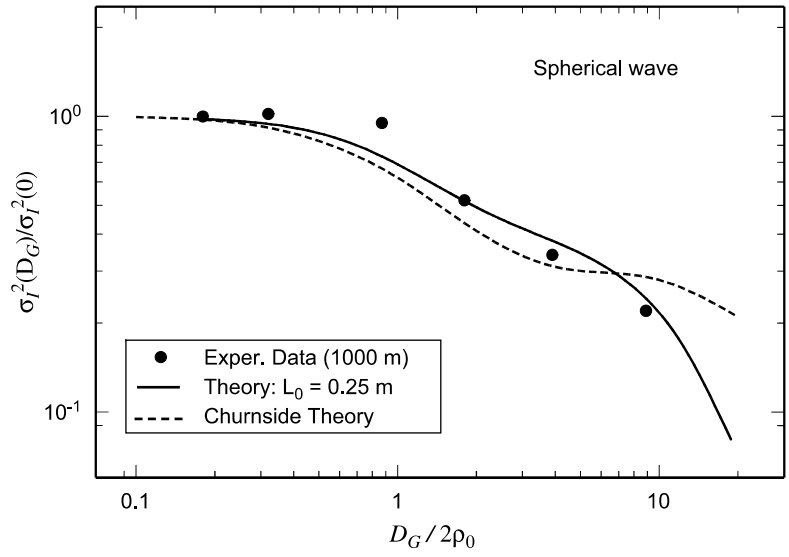

Figure 10.11 The filled circles correspond to experimental data of a spherical wave taken at 1000 m. The curve with outer-scale value is based on (71) and the dashed curve is taken from the theory of Churnside [12].

scintillation index of $\sigma_I^2(0) = 3.20$ based on nominal values of measured structure constant and inner scale provided by Churnside [12]. In Fig. 10.12 we use an outer-scale value of $L_0 = 0.35$ m leading to a scintillation index of $\sigma_I^2(0) = 3.21$, again for a 1 mm collecting lens and nominal values of measured structure constant and

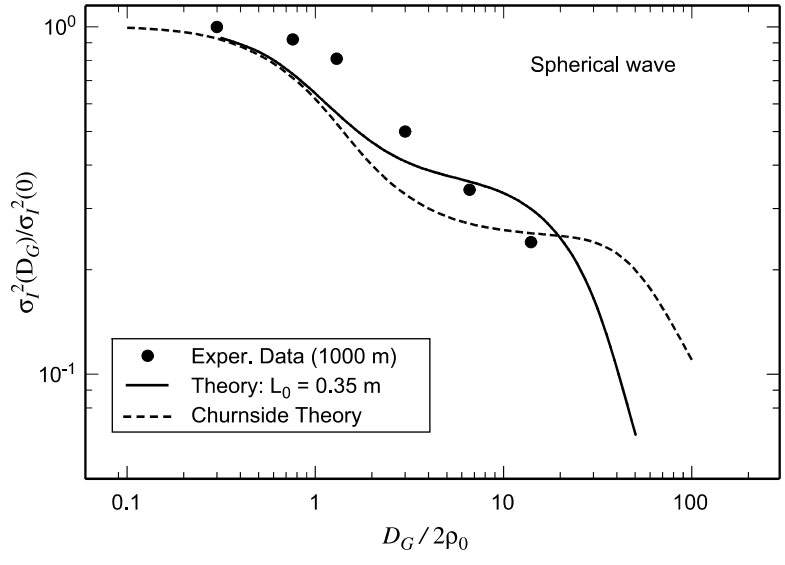

Figure 10.12 Same as Fig. 10.11 for a different data set.

inner scale. These calculated theoretical values from (71) are within the error bars of the measured data.

10.3.5 Gaussian-beam wave

In the case of a Gaussian-beam wave, the weak fluctuation expression for the irradiance flux variance obtained from Eq. (57) yields (neglecting beam wander effects)

$$\sigma_I^2(D_G) = 8\pi^2 k^2 L \int_0^1 \int_0^\infty \kappa \Phi_n(\kappa) \exp\left\{-\frac{L\kappa^2}{k(\Lambda_1 + \Omega_G)}\left[(1 - \overline{\Theta}_1\xi)^2 + \Lambda_1\Omega_G\xi^2\right]\right\} \times \left\{1 - \cos\left[\frac{L\kappa^2}{k}\left(\frac{\Omega_G - \Lambda_1}{\Omega_G + \Lambda_1}\right)\xi(1 - \overline{\Theta}_1\xi)\right]\right\} d\kappa d\xi, \quad \Omega_G \geq \Lambda_1, \tag{78}$$

where $\Omega_G = 2L/kW_G^2$ is a nondimensional parameter characterizing the spot radius of the collecting lens. Note that Eq. (78) predicts that the scintillation index vanishes when the radius of the collecting lens equals the radius of the incident wave (i.e., when $\Omega_G = \Lambda_1$).

Allowing for both inner scale and outer scale effects, the irradiance flux variance in this case leads to [16]

$$\sigma_I^2(D_G) = \exp\left[\sigma_{\ln X}^2(D_G, l_0) - \sigma_{\ln X}^2(D_G, L_0) + \sigma_{\ln Y}^2(D_G, l_0)\right] - 1, \qquad \Omega_G \geq \Lambda_1, \tag{79}$$

where

$$\sigma_{\ln X}^2(D_G, l_0) \cong 0.49\sigma_R^2\left(\frac{\Omega_G - \Lambda_1}{\Omega_G + \Lambda_1}\right)^2\left(\frac{1}{3} - \frac{1}{2}\overline{\Theta}_1 + \frac{1}{5}\overline{\Theta}_1^2\right)\left(\frac{\eta_{Xd}Q_l}{\eta_{Xd} + Q_l}\right)^{7/6} \times \left[1 + 1.75\left(\frac{\eta_{Xd}}{\eta_{Xd} + Q_l}\right)^{1/2} - 0.25\left(\frac{\eta_{Xd}}{\eta_{Xd} + Q_l}\right)^{7/12}\right], \tag{80}$$

$$\sigma_{\ln X}^2(D_G, L_0) \cong 0.49\sigma_R^2\left(\frac{\Omega_G - \Lambda_1}{\Omega_G + \Lambda_1}\right)^2\left(\frac{1}{3} - \frac{1}{2}\overline{\Theta}_1 + \frac{1}{5}\overline{\Theta}_1^2\right)\left(\frac{\eta_{Xd0}Q_l}{\eta_{Xd0} + Q_l}\right)^{7/6} \times \left[1 + 1.75\left(\frac{\eta_{Xd0}}{\eta_{Xd0} + Q_l}\right)^{1/2} - 0.25\left(\frac{\eta_{Xd0}}{\eta_{Xd0} + Q_l}\right)^{7/12}\right], \tag{81}$$

$$\sigma_{\ln Y}^2(D_G, l_0) \cong \frac{1.27\sigma_R^2\eta_Y^{-5/6}}{1 + 0.40\eta_Y/(\Lambda_1 + \Omega_G)}, \tag{82}$$

$$\eta_{Xd} = \frac{\eta_X}{1 + 0.40\eta_X(2 - \overline{\Theta}_1)/(\Lambda_1 + \Omega_G)}, \tag{83}$$

$$\eta_X = \left[\frac{0.38}{1 - 3.21\overline{\Theta}_1 + 5.29\overline{\Theta}_1^2} + 0.47\sigma_R^2 Q_l^{1/6} \left(\frac{\frac{1}{3} - \frac{1}{2}\overline{\Theta}_1 + \frac{1}{5}\overline{\Theta}_1^2}{1 + 2.20\overline{\Theta}_1} \right)^{6/7} \right]^{-1}, \quad (84)$$

$$\eta_{Xd0} = \frac{\eta_{Xd} Q_0}{\eta_{Xd} + Q_0}, \quad (85)$$

$$\eta_Y = 3(\sigma_R/\sigma_G)^{12/5}(1 + 0.69\sigma_G^{12/5}), \quad (86)$$

and where σ_G^2 is defined by Eq. (103) in Chap. 9. As before, we relate the hard aperture diameter D_G to the soft aperture (Gaussian) radius by $D_G^2 = 8W_G^2$.

In the limiting case $l_0 = 0$ and $L_0 = \infty$, the irradiance flux variance (79) reduces to

$$\sigma_I^2(D_G) = \exp\left[\sigma_{\ln X}^2(D_G) + \sigma_{\ln Y}^2(D_G)\right] - 1, \qquad \Omega_G \geq \Lambda_1, \quad (87)$$

where the large-scale and small-scale log variances take on the forms

$$\sigma_{\ln X}^2(D_G) = \frac{0.49\left(\frac{\Omega_G - \Lambda_1}{\Omega_G + \Lambda_1}\right)^2 \sigma_B^2}{\left[1 + \frac{0.4(2 - \overline{\Theta}_1)(\sigma_B/\sigma_R)^{12/7}}{(\Omega_G + \Lambda_1)\left(\frac{1}{3} - \frac{1}{2}\overline{\Theta}_1 + \frac{1}{5}\overline{\Theta}_1^2\right)^{6/7}} + 0.56(1 + \Theta_1)\sigma_B^{12/5}\right]^{7/6}}, \quad (88)$$

$$\sigma_{\ln Y}^2(D_G) = \frac{(0.51\sigma_B^2)/(1 + 0.69\sigma_B^{12/5})^{5/6}}{1 + [1.20(\sigma_R/\sigma_B)^{12/5} + 0.83\sigma_R^{12/5}]/(\Omega_G + \Lambda_1)}, \quad (89)$$

and the Rytov variance for a Gaussian beam wave is given by Eq. (91) in Chap. 9 or by its approximation for collimated and divergent beams

$$\sigma_B^2 \cong 3.86\sigma_R^2 \left\{ 0.40\left[(1 + 2\Theta_1)^2 + 4\Lambda_1^2\right]^{5/12} \times \cos\left[\frac{5}{6}\tan^{-1}\left(\frac{1 + 2\Theta_1}{2\Lambda_1}\right)\right] - \frac{11}{16}\Lambda_1^{5/6} \right\}. \quad (90)$$

In Fig. 10.13 we set $\Omega_G = 4/d^2 = 16L/kD_G^2$ and show the aperture averaging factor A as a function of scaled aperture size for various strengths of turbulence.

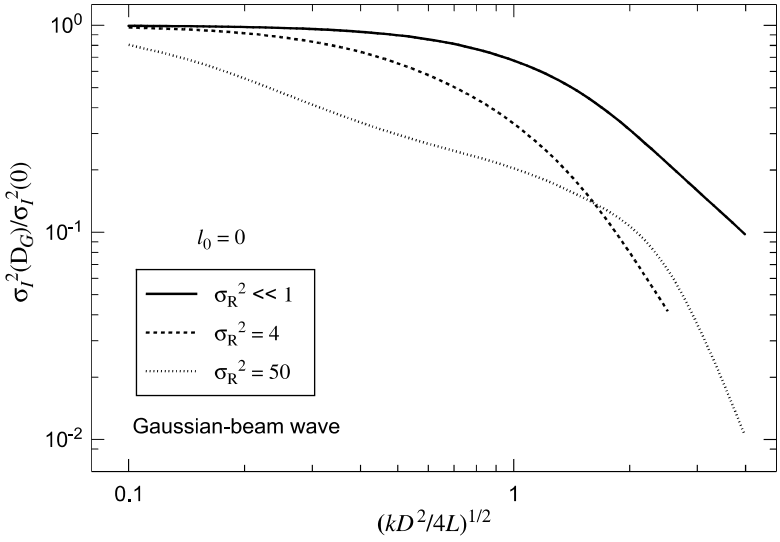

Figure 10.13 Aperture averaging factor vs. aperture radius scaled by the Fresnel zone associated with a collimated Gaussian-beam wave under various irradiance fluctuation conditions.

We take the case of a collimated beam with beam radius $W_0 = 1\,\text{cm}$ and wavelength $\lambda = 0.633\ \mu\text{m}$. Overall, the general behavior of the irradiance flux variance and aperture averaging factor A are basically the same as they are for the plane wave and spherical wave cases. Because the beam wave is of finite extent, however, the irradiance flux variance will approach zero in case where the entire beam is captured by the receiver collecting lens.

10.3.6 Temporal spectrum

In Sections 8.4 and 9.8 we discussed the temporal spectrum of irradiance fluctuations in the pupil plane of the receiver based on the frozen turbulence hypothesis of Taylor. We now wish to investigate the effect of aperture averaging on the temporal spectrum in the plane of the photodetector.

If we assume the wave incident on the receiver collecting lens is an unbounded *plane wave*, the covariance function in the plane of the photo-detector is given by

$$\begin{aligned} B_{I,\text{pl}}(\rho, D_G) &= 2\text{Re}[E_2(\mathbf{r}_1, \mathbf{r}_2) + E_3(\mathbf{r}_1, \mathbf{r}_2)] \\ &= 8\pi^2 k^2 L \int_0^1 \int_0^\infty \kappa \Phi_n(\kappa) J_0(\kappa\rho) \\ &\quad \times \exp\left(-\frac{D_G^2 \kappa^2}{16}\right)\left(1 - \cos\frac{L\kappa^2\xi}{k}\right) d\kappa\, d\xi. \end{aligned} \tag{91}$$

By setting $\rho = V_\perp \tau$, where $V_\perp$ is the transverse wind speed, this action leads to the *temporal covariance function*

$$B_I(\tau, D_G) = 8\pi^2 k^2 L \int_0^1 \int_0^\infty \kappa \Phi_n(\kappa) J_0(\kappa V_\perp \tau) \times \exp\left(-\frac{D_G^2 \kappa^2}{16}\right)\left(1 - \cos\frac{L\kappa^2 \xi}{k}\right) d\kappa\, d\xi. \tag{92}$$

Following the analysis in Section 9.8, we again write the temporal covariance function under weak-to-strong fluctuations in the form

$$B_I(\tau, D_G) = \exp[B_{\ln X}(\tau, D_G) + B_{\ln Y}(\tau, D_G)] - 1, \tag{93}$$

where $B_{\ln X}(\tau, D_G)$ and $B_{\ln Y}(\tau, D_G)$ represent the large-scale and small-scale log-irradiance covariances, respectively. For the zero inner scale case, the large-scale temporal covariance function deduced from (92) for an unbounded plane wave is

$$\begin{aligned} B_{\ln X}(\tau, D_G) &= 1.06\sigma_R^2 \int_0^1 \int_0^\infty \eta^{-11/6} \exp\left(-\frac{\eta d^2}{4} - \frac{\eta}{\eta_X}\right) \\ &\quad \times J_0(\omega_t \tau \sqrt{\eta})(1 - \cos\eta\xi) d\eta\, d\xi \\ &\cong \frac{0.49\sigma_R^2}{\left(1 + 0.65d^2 + 1.11\sigma_R^{12/5}\right)^{7/6}} {}_1F_1\left(\frac{7}{6}; 1; -\frac{\omega_t^2 \tau^2 \eta_X}{4 + d^2 \eta_X}\right), \end{aligned} \tag{94}$$

and the small-scale log-irradiance temporal covariance is likewise given by

$$\begin{aligned} B_{\ln Y}(\tau, D_G) &= 1.06\sigma_R^2 \int_0^1 \int_0^\infty \exp\left(-\frac{\eta d^2}{4}\right) \frac{J_0(\omega_t \tau \sqrt{\eta})}{(\eta + \eta_Y)^{11/6}} (1 - \cos\eta\xi) d\eta\, d\xi \\ &\cong \frac{0.51\sigma_R^2 \left(1 + 0.69\sigma_R^{12/5}\right)^{-5/6}}{1 + 0.90d^2 + 0.62d^2\sigma_R^{12/5}} (\omega_t^2 \tau^2 \eta_Y)^{5/12} K_{5/6}(\omega_t \tau \sqrt{\eta_Y}), \end{aligned} \tag{95}$$

where $\omega_t = V_\perp / \sqrt{L/k}$, ${}_1F_1(a; c; x)$ is a confluent hypergeometric function, and $K_\nu(x)$ is a modified Bessel function of the second kind. The quantity ω_t physically represents the transition frequency at which the spectrum begins to decay under weak fluctuations.

By using (93)–(95), the resulting *temporal spectrum of irradiance fluctuations* can be deduced from the Fourier transform relation

$$S_I(\omega, D_G) = 4 \int_0^\infty B_I(\tau, D_G) \cos\omega\tau d\tau, \tag{96}$$

which, following the change of variable $s = \omega_t \tau$, yields the more useful form

$$S_I(\omega, D_G) = \frac{4}{\omega_t} \int_0^\infty B_I(s/\omega_t, D_G) \cos\left(\frac{\omega s}{\omega_t}\right) ds. \tag{97}$$

In Figs. 10.14–10.16 we show numerical evaluations of the quantity $\omega S_I(\omega, D_G)$, scaled by $2\pi\sigma_I^2(D_G)$, as a function of ω/ω_t and various aperture diameters for the

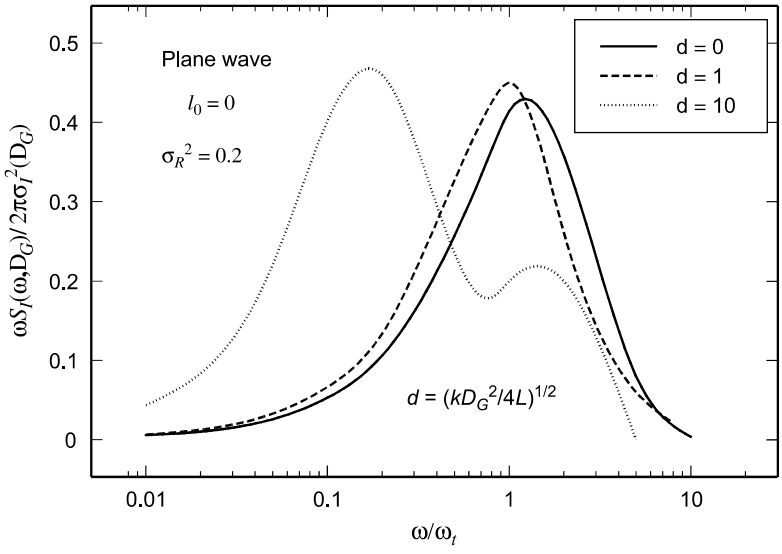

Figure 10.14 Scaled temporal power spectrum of a plane wave in the focal plane of a lens plotted as a function of radial frequency scaled by the quantity $\omega_t = V_\perp/\sqrt{(L/k)}$, where $V_\perp$ is transverse wind speed. The irradiance fluctuations are weak.

case of zero inner scale. By plotting the spectrum in this fashion, we obtain a clear representation of power content, viz., which frequencies (scale sizes) contribute most to the power of irradiance fluctuations for different aperture sizes of the receiver collecting lens.

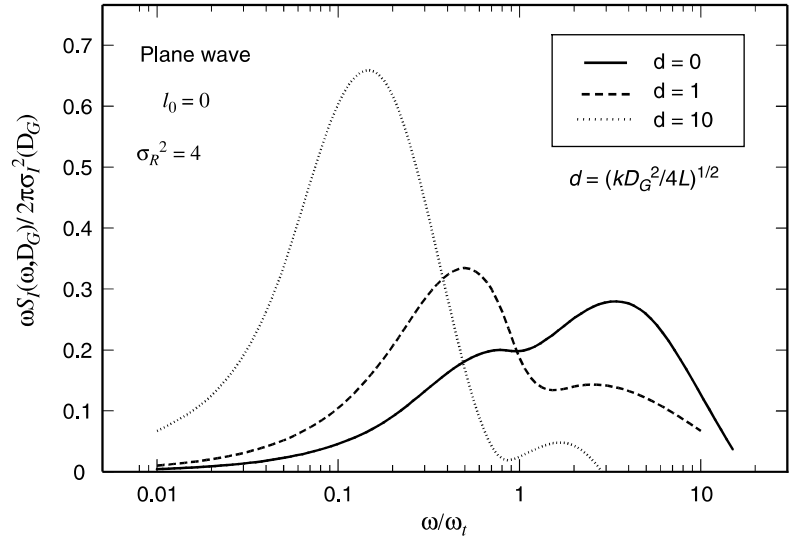

Figure 10.15 Same as Fig. 10.14 except that the irradiance fluctuations are moderate, corresponding to the following regime.

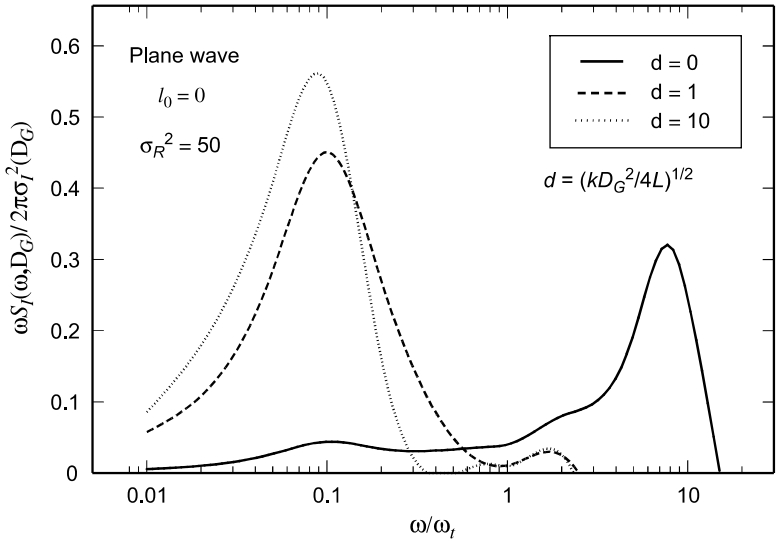

Figure 10.16 Same as Fig. 10.14 except that the irradiance fluctuations correspond to the saturation regime.

The curves illustrated in Fig. 10.14 correspond to weak fluctuation conditions ($\sigma_R^2 = 0.2$). The irradiance correlation width of the incident plane wave under weak fluctuation conditions is the Fresnel zone, so power concentration for a point aperture ($D_G = 0$) is centered at $\omega_t = V_\perp/\sqrt{L/k}$. For aperture sizes commensurate with the correlation width, i.e., $\sqrt{kD_G^2/4L} = 1$, there is little transfer of power to lower frequencies because no appreciable amount of aperture averaging takes place. However, for $\sqrt{kD_G^2/4L} = 10$ there is appreciable aperture averaging which accounts for the significant shift in power concentration to lower frequencies. The secondary concentration of power near $\omega/\omega_t = 1$ in this latter case shows that there is still some power left in the small scales near Fresnel zone size.

In Fig. 10.15 the curves represent the focusing regime ($\sigma_R^2 = 4$) for the incident plane wave. Here the Fresnel zone, transverse spatial coherence radius, and scattering disk are all of similar size. Nonetheless, for the point aperture case the largest concentration of power occurs for $\omega \sim 3\omega_t$ but there is a secondary concentration at lower frequencies corresponding to the large scales. For the curve representing $\sqrt{kD_G^2/4L} = 1$, the shift in power concentration is reversed from the point aperture case, with the greatest power concentration in the lower frequencies. As in Fig. 10.14, almost all of the power has shifted to low frequencies in the large aperture case $\sqrt{kD_G^2/4L} = 10$.

The curves in Fig. 10.16 correspond to the saturation regime ($\sigma_R^2 = 50$). In the point aperture case nearly all the power is concentrated in the high frequencies $\omega \gg \omega_t$ defined by scale sizes on the order of the spatial coherence radius. Unlike previous cases in Figs. 10.14 and 10.15, here we notice that aperture sizes on the order of the Fresnel zone lead to substantial amounts of aperture

averaging as evidenced by the large shift in power concentration to lower frequencies for $\sqrt{kD_G^2/4L} = 1$. In fact, there is little additional shift in power concentration for the largest aperture size depicted in Fig. 10.16 as a consequence of the leveling effect of the aperture averaging factor illustrated in Fig. 10.7 for aperture sizes in which $\sqrt{kD_G^2/4L} \sim 1 - 10$.

Lastly, although we don't show it, the presence of an inner scale and/or outer scale will change the peak values of the curves shown in Figs. 10.14–10.16, but not significantly shift the location of the peak values.

10.4 Optical Systems with Several Optical Elements

The general complex optical system to be considered in this section is shown in Fig. 10.17, consisting of N optical elements distributed arbitrarily between input and output planes. Although the resulting expressions for the statistical moments of interest are quite complex for such systems, it is a straightforward procedure to generalize the results for one optical element to the optical system in Fig. 10.17.[1] For example, if Θ_m and Λ_m denote the beam parameters at O_m for the beam propagating from optical element O_{m-1} to O_m, the on-axis amplitude of the beam at the output plane in the absence of a random medium can be represented by the product

$$\frac{1}{p(L)} = \Pi_{m=1}^{N+1}(\Theta_m - i\Lambda_m) = \Theta - i\Lambda, \tag{98}$$

where $L = L_1 + L_2 + \cdots + L_{N+1}$.

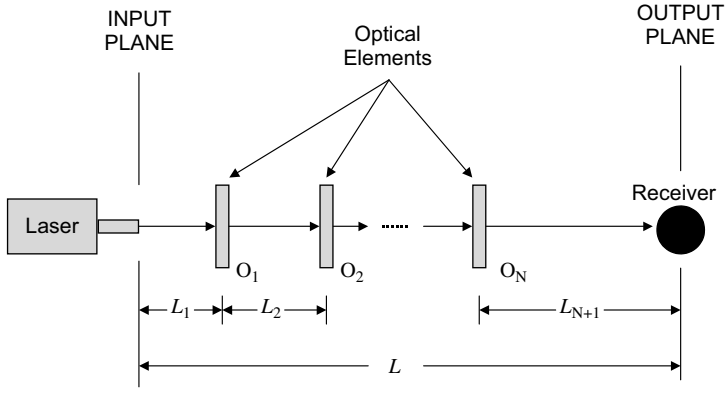

Figure 10.17 Schematic representation of optical wave propagation through a general propagation system consisting of a train of optical element O_1, O_2, ..., O_N arbitrarily located along the propagation path.

[1]As before, we are ignoring the thickness of each optical element.

If the total path length from the input plane to output plane is divided into subintervals at each optical element, the spectral representation for ψ_1 leads to the sum

$$\psi_1(\mathbf{r}, L) = ik \sum_{m=1}^{N+1} \int_0^{L_m} \int\int_{-\infty}^{\infty} \exp\left[i\gamma_m \mathbf{K} \cdot \mathbf{r} - \frac{i\kappa^2 \gamma_m}{2k} B(z_m; L - \zeta_{m-1}) \right] d\nu\,(\mathbf{K}, z_m) dz_m, \tag{99}$$

where γ_m denotes the path amplitude ratio between optical elements O_{m-1} and O_m, and

$$\zeta_0 = 0, \quad \zeta_m = \sum_{j=1}^{m} L_j, \qquad m = 1, 2, \ldots, N. \tag{100}$$

Owing to the statistical independence of each link of the random medium between optical elements, the moments E_2 and E_3 are given by

$$\begin{aligned} E_2(\mathbf{r}_1, \mathbf{r}_2) &= \langle \psi_1(\mathbf{r}_1, L) \psi_1^*(\mathbf{r}_2, L) \rangle \\ &= 2\pi k^2 \sum_{m=1}^{N+1} \int_0^{L_m} \int\int_{-\infty}^{\infty} \Phi_n(\mathbf{K}, z_m) \exp\left\{ i\mathbf{K} \cdot (\gamma_m \mathbf{r}_1 - \gamma_m^* \mathbf{r}_2) - \frac{i\kappa^2}{2k} \right. \\ &\quad \left. \times \left[\gamma_m B(z_m; L - \zeta_{m-1}) - \gamma_m^* B^*(z_m; L - \zeta_{m-1}) \right] \right\} d^2\kappa\, dz_m, \end{aligned} \tag{101}$$

$$\begin{aligned} E_3(\mathbf{r}_1, \mathbf{r}_2) &= \langle \psi_1(\mathbf{r}_1, L) \psi_1(\mathbf{r}_2, L) \rangle \\ &= -2\pi k^2 \sum_{m=1}^{N+1} \int_0^{L_m} \int\int_{-\infty}^{\infty} \Phi_n(\mathbf{K}, z_m) \exp\left[i\gamma_m \mathbf{K} \cdot (\mathbf{r}_1 - \mathbf{r}_2) \right. \\ &\quad \left. - \frac{i\kappa^2}{k} \gamma_m B(z_m; L - \zeta_{m-1}) \right] d^2\kappa dz_m. \end{aligned} \tag{102}$$

From these general expressions and Eq. (15) in Chap. 6 for $E_1(0, 0)$, all second-order statistical moments can be determined for one-way propagation through general paraxial optical systems.

10.4.1 Two optical elements

As a specific case of an optical system with more than one optical element, let us consider the system illustrated in Fig. 10.18 featuring two thin (Gaussian) lenses. We characterize the first lens by the complex parameter

$$\alpha_G = \frac{2}{kW_G^2} + i\frac{1}{F_G}, \tag{103}$$

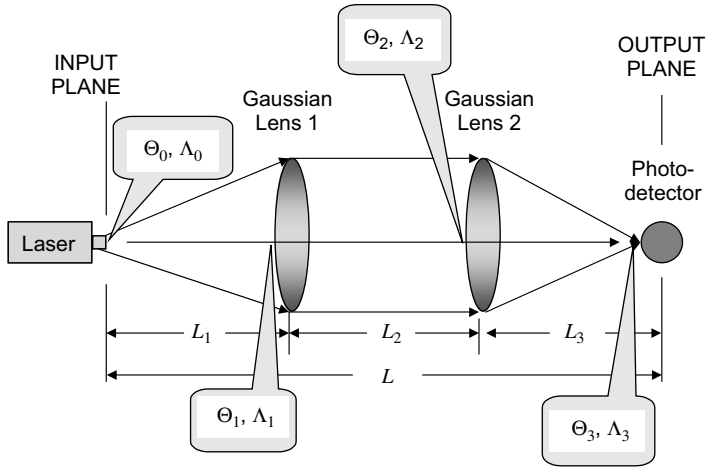

Figure 10.18 Propagation geometry for a Gaussian beam originating at distance L_1 to the left of a thin Gaussian lens followed by a second thin lens at distance L_2 from the first lens, both having finite effective transmission radii.

where W_G and F_G denote the finite aperture radius and focal length, and in the same fashion for the second lens we write

$$\alpha_g = \frac{2}{kW_g^2} + i\frac{1}{F_g}, \tag{104}$$

where W_g and F_g are the corresponding finite aperture radius and focal length.

The overall *ABCD* matrix for the optical system shown in Fig. 10.18 is described by

$$\begin{aligned}\begin{pmatrix} A & B \\ C & D \end{pmatrix} &= \begin{pmatrix} 1 & L_3 \\ 0 & 1 \end{pmatrix}\begin{pmatrix} 1 & 0 \\ i\alpha_g & 1 \end{pmatrix}\begin{pmatrix} 1 & L_2 \\ 0 & 1 \end{pmatrix}\begin{pmatrix} 1 & 0 \\ i\alpha_G & 1 \end{pmatrix}\begin{pmatrix} 1 & L_1 \\ 0 & 1 \end{pmatrix} \\ &= \begin{pmatrix} a_2 + (c_2 + i\alpha_g a_2)L_3 & b_2 + (d_2 + i\alpha_g b_2)L_3 \\ c_2 + i\alpha_g a_2 & d_2 + i\alpha_g b_2 \end{pmatrix},\end{aligned} \tag{105}$$

where a_2, b_2, c_2, and d_2 are matrix elements that describe the propagation path up to the second lens. These elements are defined by

$$\begin{aligned}\begin{pmatrix} a_2 & b_2 \\ c_2 & d_2 \end{pmatrix} &= \begin{pmatrix} 1 & L_2 \\ 0 & 1 \end{pmatrix}\begin{pmatrix} 1 & 0 \\ i\alpha_G & 1 \end{pmatrix}\begin{pmatrix} 1 & L_1 \\ 0 & 1 \end{pmatrix} \\ &= \begin{pmatrix} 1 + i\alpha_G L_2 & L_1 + L_2(1 + i\alpha_G L_1) \\ i\alpha_G & 1 + i\alpha_G L_1 \end{pmatrix}.\end{aligned} \tag{106}$$

From the expression (105) we calculate the propagation parameter

$$\begin{aligned}p(L) &= A(L) + i\alpha_0 B(L) \\ &= a_2 + (c_2 + i\alpha_g a_2)L_3 + i\alpha_0[b_2 + (d_2 + i\alpha_g b_2)L_3],\end{aligned} \tag{107}$$

which can be used to generate the beam parameters

$$\frac{1}{p(L)} = \Theta - i\Lambda = (\Theta_1 - i\Lambda_1)(\Theta_2 - i\Lambda_2)(\Theta_3 - i\Lambda_3). \tag{108}$$

In this case, parameters Θ, Λ denote the real and imaginary parts of the product of complex quantities on the right in (108). Also, parameters Θ_1, Λ_1 and Θ_2, Λ_2 are the same as defined by (8) and (9), whereas parameters Θ_0, Λ_0 are those defined by (7) to characterize the spot radius W_0 and phase front radius of curvature F_0 of the Gaussian-beam wave at the input plane. For the development of the third set of beam parameters, we find it convenient here to use a somewhat different approach than relying directly on (107) and (108). First, we characterize the beam emerging from the lead Gaussian lens in Fig. 10.18 by the beam radius and phase front radius of curvature $\hat{W}_1$ and $\hat{F}_1$, respectively, which are defined by

$$\frac{1}{\hat{W}_1^2} = \frac{1}{W_1^2} + \frac{1}{W_G^2}, \qquad \frac{1}{\hat{F}_1} = \frac{1}{F_1} + \frac{1}{F_G}. \tag{109}$$

We can then characterize the beam emerging from the first lens by introducing the additional beam parameters

$$\begin{aligned} \hat{\theta}_1 &= 1 - \frac{L_2}{\hat{F}_1} = \frac{L_2}{L_1}\left(\frac{L_1}{L_2} - \frac{L_1}{F_G} + \overline{\Theta}_1\right), \\ \hat{\lambda}_1 &= \frac{2L_2}{k\hat{W}_1^2} = \frac{L_2}{L_1}(\Lambda_1 + \Omega_G). \end{aligned} \tag{110}$$

The remaining propagation path between the first lens and output plane now corresponds with the propagation path depicted in Fig. 10.1 featuring a single lens, except distances L_1 and L_2 in Fig. 10.1 are now L_2 and L_3. Hence, the beam incident on the second lens is characterized by

$$\begin{aligned} \Theta_2 &= \frac{\hat{\theta}_1}{\hat{\theta}_1^2 + \hat{\lambda}_1^2} = \frac{L_1}{L_2}\left[\frac{L_1/L_2 - L_1/F_G + \overline{\Theta}_1}{(L_1/L_2 - L_1/F_G + \overline{\Theta}_1)^2 + (\Lambda_1 + \Omega_G)^2}\right], \\ \Lambda_2 &= \frac{\hat{\lambda}_1}{\hat{\theta}_1^2 + \hat{\lambda}_1^2} = \frac{L_1}{L_2}\left[\frac{\Lambda_1 + \Omega_G}{(L_1/L_2 - L_1/F_G + \overline{\Theta}_1)^2 + (\Lambda_1 + \Omega_G)^2}\right], \end{aligned} \tag{111}$$

which is in agreement with Eqs. (9). Beam characteristics at the output plane are therefore described by the beam parameters

$$\begin{aligned} \Theta_3 &= \frac{L_2}{L_3}\left[\frac{L_2/L_3 - L_2/F_g + \overline{\Theta}_2}{(L_2/L_3 - L_2/F_g + \overline{\Theta}_2)^2 + (\Lambda_2 + \Omega_g)^2}\right], \\ \Lambda_3 &= \frac{L_2}{L_3}\left[\frac{\Lambda_2 + \Omega_g}{(L_2/L_3 - L_2/F_g + \overline{\Theta}_2)^2 + (\Lambda_2 + \Omega_g)^2}\right]. \end{aligned} \tag{112}$$

If we assume optical turbulence exists everywhere along the propagation path and follow our approach in Section 10.2, we deduce that

$$
\begin{aligned}
E_1(0,0) = &-2\pi^2 k^2 L_1 \int_0^1 \int_0^\infty \kappa \Phi_n(\kappa) d\kappa d\xi - 2\pi^2 k^2 L_2 \int_0^1 \int_0^\infty \kappa \Phi_n(\kappa)\, d\kappa\, d\xi \\
&- 2\pi^2 k^2 L_3 \int_0^1 \int_0^\infty \kappa \Phi_n(\kappa)\, d\kappa\, d\xi, \qquad (113)
\end{aligned}
$$

$$
\begin{aligned}
E_2(\mathbf{r}_1, \mathbf{r}_2) = &\, 4\pi^2 k^2 L_1 \int_0^1 \int_0^\infty \kappa \Phi_n(\kappa) J_0\big(\kappa |\gamma_1 \mathbf{r}_1 - \gamma_1^* \mathbf{r}_2|\big) \\
&\times \exp\left\{ -\frac{i\kappa^2}{2k} \big[\gamma_1 B_1(\xi) - \gamma_1^* B_1^*(\xi)\big] \right\} d\kappa\, d\xi \\
&+ 4\pi^2 k^2 L_2 \int_0^1 \int_0^\infty \kappa \Phi_n(\kappa) J_0\big(\kappa |\gamma_2 \mathbf{r}_1 - \gamma_2^* \mathbf{r}_2|\big) \\
&\times \exp\left\{ -\frac{i\kappa^2}{2k} \big[\gamma_2 B_2(\xi) - \gamma_2^* B_2^*(\xi)\big] \right\} d\kappa\, d\xi \qquad (114) \\
&+ 4\pi^2 k^2 L_3 \int_0^1 \int_0^\infty \kappa \Phi_n(\kappa) J_0\big(\kappa |\gamma_3 \mathbf{r}_1 - \gamma_3^* \mathbf{r}_2|\big) \\
&\times \exp\left\{ -\frac{i\kappa^2}{2k} \big[\gamma_3 B_3(\xi) - \gamma_3^* B_3^*(\xi)\big] \right\} d\kappa\, d\xi,
\end{aligned}
$$

$$
\begin{aligned}
E_3(\mathbf{r}_1, \mathbf{r}_2) = &-4\pi^2 k^2 L_1 \int_0^1 \int_0^\infty \kappa \Phi_n(\kappa) J_0\big(\gamma_1 \kappa \rho\big) \exp\left[-\frac{i\kappa^2}{k} \gamma_1 B_1(\xi) \right] d\kappa\, d\xi \\
&- 4\pi^2 k^2 L_2 \int_0^1 \int_0^\infty \kappa \Phi_n(\kappa) J_0\big(\gamma_2 \kappa \rho\big) \exp\left[-\frac{i\kappa^2}{k} \gamma_2 B_2(\xi) \right] d\kappa\, d\xi \qquad (115) \\
&- 4\pi^2 k^2 L_3 \int_0^1 \int_0^\infty \kappa \Phi_n(\kappa) J_0\big(\gamma_3 \kappa \rho\big) \exp\left[-\frac{i\kappa^2}{k} \gamma_3 B_3(\xi) \right] d\kappa\, d\xi.
\end{aligned}
$$

The parameters γ_1, γ_2, and γ_3 are defined, respectively, by

$$
\begin{aligned}
0 < z < L_1: &\quad \gamma_1 = \frac{p(z)}{p(L)}, \\
L_1 < z < L_2: &\quad \gamma_2 = \frac{p(z)}{p(L)}, \qquad (116) \\
L_2 < z < L_3: &\quad \gamma_3 = \frac{p(z)}{p(L)},
\end{aligned}
$$

and the corresponding matrix terms $B_1(\xi), B_2(\xi)$, and $B_3(\xi)$ can be derived by considering the optical wave propagating backward from the output plane to

position z. However, in a number of practical cases, the second lens may be part of a receiver system and hence, optical turbulence can be neglected over the short distance denoted by L_3. We leave the general evaluations of calculating these quantities in terms of the various beam parameters to the exercises (see Probs. 14 and 15).

10.5 Summary and Discussion

In this chapter we extended the theory presented in Chaps. 6 through 9 for line-of-sight propagation to include the placement of (perfectly aligned) optical elements arbitrarily distributed along the propagation path. Our approach is based on rotationally symmetric paraxial optical systems that can be represented by *ABCD* ray matrices. We assume that the input and output planes are in the same medium so that $AD - BC = 1$.

For the case of a thin lens at distance L_1 from the transmitter with focal length F_{G} and Gaussian limiting aperture radius W_G, we find it useful to introduce three sets of nondimensional *beam parameters*—one set Θ_0, Λ_0 depicting beam characteristics F_0, W_0 at the transmitter in terms of the propagation distance L_1; another set Θ_1, Λ_1 depicting beam characteristics F_1, W_1 of the optical wave incident on the lens in terms of L_1; and a third set Θ_2, Λ_2 characterizing $F_2 = F, W_2 = W$ of the optical wave in the plane of the receiver in terms of propagation distance L_2 between the lens and the output plane. In all cases, $F_n, n = 0, 1, 2$ denotes the phase front radius of curvature of the beam and $W_n, n = 0, 1, 2$ is the spot radius.

A particular application of the single lens system discussed here includes the case when the input and output planes are in the front and back focal planes of the lens. In this setting we have $L_1 = L_2 = F_G$ and obtain the geometric configuration known as the *Fourier-transform plane*. Another example of a single lens system is used in imaging applications (see also Chap. 14). The *ABCD* matrix technique permits a simple evaluation of the ratio of on-axis mean irradiance to that in the absence of turbulence known as the *Strehl ratio*, a parameter commonly used as a measure of system performance. The above beam parameters are also valid for the case when the Gaussian lens is replaced by a Gaussian mirror that reflects the wave back to the input plane with $L_1 = L_2 = L$ (see Chap. 13).

Aperture averaging takes place when a large-aperture receiver lens is used to focus the collected light onto a photodetector for processing. For small receiving apertures, much of the power in the irradiance fluctuations is concentrated at high frequencies. Under weak irradiance fluctuations, for example, the power is concentrated near the Fresnel frequency $\omega_t = V_\perp/\sqrt{L/k}$, where $V_\perp$ is the average transverse wind speed, but under strong irradiance fluctuations the power is concentrated at even higher frequencies. As the receiver aperture diameter begins to increase, the greatest power concentration always shifts to lower frequencies although there may still exist a secondary concentration at the higher frequencies. Basically, this is a two-scale phenomenon that we interpret to mean that small-scale scintillation is reduced first as the receiver aperture is increased, and upon reaching a sufficient size, the large-scale scintillation may then also decrease.

The *irradiance flux variance* on the photodetector surface behind a large receiver aperture can be approximated more readily by the *ABCD* method illustrated here than by conventional methods utilizing the modulation transfer function (MTF) of the optical system and covariance function of irradiance in the pupil plane. In particular, in the case of a *Gaussian-beam wave* at the transmitter, the traditional plane wave and spherical wave aperture averaging results are readily deduced from our more general expression for the Gausssian beam.

10.6 Worked Examples

Example 1: Consider a spherical wave of wavelength $\lambda = 0.633\ \mu\text{m}$ at the transmitter of an imaging system. If a thin Gaussian lens with $W_G = 1$ cm is placed at the end of the path $L_1 = 1200$ m where the refractive-index structure parameter is $C_n^2 = 10^{-14}\,\text{m}^{-2/3}$ and the signal is detected at distance $L_2 = 10\,\text{cm}$ behind the lens, calculate at this point the

(*a*) effective focal length of the lens,
(*b*) free-space spot radius, and
(*c*) effective spot radius.

Solution: We first calculate the parameters:

$$\Theta_1 = 0, \quad \Lambda_1 = 0, \quad \Omega_G = \frac{2L_1}{kW_G^2} = 2.4179,$$

$$\Theta_2 = 0, \quad \Lambda_2 = \frac{L_1}{L_2\Omega_G} = 4963, \quad \sigma_R^2 = 1.23C_n^2k^{7/6}L_1^{11/6} = 0.791.$$

(*a*) $F_G = \dfrac{L_1L_2}{L_1 + L_2} = 9.999\,\text{cm}$

(*b*) $W = \dfrac{2L_2}{kW_G} = 2.01\ \mu\text{m}$

(*c*) $W_{\text{LT}} = W\sqrt{1 + 1.33\sigma_R^2\Omega^{-5/6}} = 2.47\ \mu\text{m}$

❑

Example 2: A spherical wave is propagated through atmospheric turbulence to a receiver located 500 meters from the transmitter. Given that the wavelength is 0.5 μm and $C_n^2 = 0.5 \times 10^{-13}\,\text{m}^{-2/3}$,

(*a*) calculate the scintillation index at the pupil plane of the receiver.
(*b*) If the receiver aperture is 4 cm in diameter, calculate the flux variance (reduced scintillation) in the plane of the detector.
(*c*) If the propagation distance is 1.5 km, what is the scintillation index and flux variance given the same wavelength and receiver aperture diameter?

(*d*) If the propagation distance is 5 km, the wavelength is increased to 1.5 μm, and the receiver aperture diameter is increased to 10 cm, what is the scintillation index and corresponding flux variance?

Solution: We first calculate parameters:

$$L = 500\,\text{m}: \quad \beta_0^2 = 0.5C_n^2 k^{7/6} L^{11/6} = 0.425, \quad d = \sqrt{\frac{kD_G^2}{4L}} = 3.17$$

$$L = 1500\,\text{m}: \quad \beta_0^2 = 3.186, \quad d = 1.83$$

$$L = 5000\,\text{m}: \quad \beta_0^2 = 8.038, \quad d = 1.45$$

$$(a) \quad \sigma_I^2 = \exp\left[\frac{0.49\beta_0^2}{\left(1 + 0.56\beta_0^{12/5}\right)^{7/6}} + \frac{0.51\beta_0^2}{\left(1 + 0.69\beta_0^{12/5}\right)^{5/6}}\right] - 1 = 0.42$$

$$(b) \quad \sigma_I^2(D_G) = \exp\left[\frac{0.49\beta_0^2}{\left(1 + 0.18d^2 + 0.56\beta_0^{12/5}\right)^{7/6}} + \frac{0.51\beta_0^2(1 + 0.69\beta_0^{12/5})^{-5/6}}{1 + 0.90d^2 + 0.62d^2\beta_0^{12/5}}\right] - 1 = 0.07$$

(*c*) $\sigma_I^2 = 1.54, \qquad \sigma_I^2(D_G) = 0.44$

(*d*) $\sigma_I^2 = 1.69, \qquad \sigma_I^2(D_G) = 0.45$

❑

Example 3: A spherical wave propagates along a horizontal path a distance of 2500 m to a receiver. If the wavelength is 1.55 μm, what receiver aperture size is required to reduce the flux variance to a level of 0.1 or less? Assume turbulence is governed by a Kolmogorov spectrum and that $C_n^2 = 0.57 \times 10^{-13}\,\text{m}^{-2/3}$.

Solution: We first calculate the spherical wave Rytov variance

$$\beta_0^2 = 0.5C_n^2 k^{7/6} L^{11/6} = 2.47.$$

Then, by trial and error, we deduce that with $D_G = 30\,\text{cm}$, the flux variance is

$$\sigma_I^2(D_G) = \exp\left[\frac{0.49\beta_0^2}{(1 + 0.18d^2 + 0.56\beta_0^{12/5})^{7/6}} + \frac{0.51\beta_0^2(1 + 0.69\beta_0^{12/5})^{-5/6}}{1 + 0.90d^2 + 0.62d^2\beta_0^{12/5}}\right] - 1$$
$$= 0.10.$$

Consequently, any receiver aperture that is 30 cm or more will reduce the flux variance to an acceptable level.

❑

Problems

Section 10.2

1. Given $0 < z < L_1$ and $(L = L_1 + L_2)$

$$p(z) = A(z) + i\alpha_0 B(z) = 1 + i\alpha_0 L_1(1 - \xi),$$
$$p(L) = A(L) + i\alpha_0 B(L) = 1 + i\alpha_G L_2 + i\alpha_0 L_1 + i\alpha_0 L_2(1 + i\alpha_G L_1),$$

show that

$$\gamma_1 = \frac{p(z)}{p(L)} = (\Theta - i\Lambda)\xi + (\Theta_2 - i\Lambda_2)(1 - \xi), \qquad 0 \le \xi \le 1,$$

where $\Theta \pm i\Lambda = (\Theta_1 \pm i\Lambda_1)(\Theta_2 \pm i\Lambda_2)$.
Hint: Recall Eqs. (120) and (121) in Chap. 4.

2. Given $L_1 < z < L$ and $(L = L_1 + L_2)$

$$p(z) = A(z) + i\alpha_0 B(z) = 1 + i\alpha_G L_2\eta + i\alpha_0 L_1 + i\alpha_0 L_2(1 + i\alpha_G L_1)\eta,$$
$$p(L) = A(L) + i\alpha_0 B(L) = 1 + i\alpha_G L_2 + i\alpha_0 L_1 + i\alpha_0 L_2(1 + i\alpha_G L_1),$$

show that $(z' = z - L_1)$

$$\gamma_2 = \frac{p(L_1 + z')}{p(L_1 + L_2)}$$

$$= -(\Theta - i\Lambda)L_2\eta/L_1 + (\Theta_2 - i\Lambda_2)(1 + L_2\eta/L_1 + i\alpha_G L_2\eta), \quad 0 \le \eta \le 1,$$

where $\Theta \pm i\Lambda = (\Theta_1 \pm i\Lambda_1)(\Theta_2 \pm i\Lambda_2)$.
Hint: Recall Eqs. (120) and (121) in Chap. 4.

3. A point source (spherical wave) is located 1 km from a collecting lens of diameter 1 cm and focal length 4 cm. Given that $\lambda = 1.06\ \mu\text{m}$ and $C_n^2 = 5 \times 10^{-14}\ \text{m}^{-2/3}$,
   (*a*) Calculate the free-space spot size in the focal plane of the lens.
   (*b*) Use the Kolmogorov spectrum to calculate the effective spot size in the focal plane of the lens.
   (*c*) Use the Kolmogorov spectrum to calculate the scintillation index in the focal plane of the lens.

4. Consider the geometry in which the Gaussian lens in Fig. 10.1 is located midway between input and output planes, i.e., $L_1 = L_2 = L$ for a total propagation distance of $2L$.
   (*a*) For an incident spherical wave, show that the wave emerging from the lens is a Gaussian-beam wave with beam radius $W_0 = W_G$ and phase front radius of curvature $1 \neq F_0 = 1/F_G - 1/L$, where W_G and F_G denote the finite aperture radius and focal length, respectively, of the lens.
   (*b*) Under the conditions stated above, assume that a random medium exists only between the Gaussian lens and the output plane and show

that the resulting expressions for moments $E_2(\mathbf{r}_1,\mathbf{r}_2)$ and $E_3(\mathbf{r}_1,\mathbf{r}_2)$ are equivalent to those given by Eqs. (22) and (23) in Chap. 6 for the line-of-sight propagation of a Gaussian-beam wave.

5. The *optical transfer function* (OTF) is defined as the normalized two-dimensional spatial Fourier transform of the mean *point spread function* (PSF), or mean irradiance in the image plane of a point source (see also Section 14.3). By writing the mean irradiance (46) as

$$\langle I(\mathbf{r},L)\rangle = \frac{\pi^2 D_G^4}{64\lambda^2 f^2\left[1+(D_G/r_0)^{5/3}\right]} \times \exp\left\{-\frac{\pi^2 D_G^2 r^2}{4\lambda^2 f^2\left[1+(D_G/r_0)^{5/3}\right]}\right\}, \qquad L_1 \gg L_2 = f,$$

where D_G is the diameter of the telescope lens, f is its focal length, r_0 is the atmospheric coherence width, and λ is wavelength,

(*a*) show that the modulus of the OTF or *modulation transfer function* (MTF) is

$$\begin{aligned}\mathrm{MTF}(\nu) &= |\mathrm{OTF}(\nu)| \\ &= \exp\left[-4\left(\frac{\lambda f\nu}{D_G}\right)^2\right]\exp\left[-4\left(\frac{\lambda f\nu}{D_G}\right)^{1/3}\left(\frac{\lambda f\nu}{r_0}\right)^{5/3}\right],\end{aligned}$$

where the first exponential function represents the MTF of the lens and the second exponential function is the atmospheric MTF in weak turbulence.

(*b*) The *resolution* of an imaging system is defined as the volume under the MTF surface (Section 14.3). Based on the result of part (*a*), deduce that

$$R = \frac{\pi D_G^2}{4\lambda^2 f^2[1+(D_G/r_0)^{5/3}]}, \qquad D_G < r_0.$$

6. Given that the maximum resolution of an imaging system under weak fluctuations is $R_{\max} = (D_G \neq r_0)^{1/3}$

(*a*) use the result of Prob. 5 to deduce that

$$\frac{R}{R_{\max}} = \frac{(D_G/r_0)^{5/3}}{1+(D_G/r_0)^{5/3}}, \qquad D_G < r_0.$$

(*b*) For sufficiently small telescopes such that $D_G/r_0 \ll 1$, show that the result in (*a*) reduces to

$$\frac{R}{R_{\max}} \cong \left(\frac{D_G}{r_0}\right)^{5/3}, \qquad \frac{D_G}{r_0} \ll 1.$$

(*c*) Plot the ratio in (*a*) and that given by the first expression in (30) in Chap. 14 as a function of D_G/r_0, $0 \le D_G/r_0 \le 5$. What is the

percentage difference in numerical results for the two expressions when $D_G/r_0 = 1$, $D_G/r_0 = 2$, and $D_G/r_0 = 5$?

7. Given Eq. (51) for the scintillation index in the image plane of a point source, use the Kolmogorov spectrum to deduce the *aperture-averaging factor* (53) for a spherical wave.

Section 10.3

8. For an infinite plane wave in the absence of inner and outer scale effects,
   (*a*) use the large-scale filter function in Section 9.41 to deduce that

$$\sigma^2_{\ln X}(D_G) = 1.06\sigma_R^2\left(\frac{L}{k}\right)^{7/6}\int_0^1 \xi^2 d\xi \int_0^\infty \kappa^{4/3}\exp\left[-\frac{\kappa^2}{\kappa_X^2}\left(1+\frac{d^2\eta_X}{4}\right)\right]d\kappa$$

$$= \frac{0.16\sigma_R^2\eta_X^{7/6}}{\left(1+d^2\eta_X/4\right)^{7/6}}, \qquad d = \sqrt{\frac{kD_G^2}{4L}}.$$

   (*b*) Use the small-scale filter function defined in Section 9.41 to deduce that

$$\sigma^2_{\ln Y}(D_G) = 1.06\sigma_R^2\int_0^\infty \frac{1}{(\eta+\eta_Y)^{11/6}}\exp\left(-\frac{d^2\eta}{4}\right)d\eta$$

$$\cong \frac{1.27\sigma_R^2\eta_Y^{-5/6}}{1+0.3d^2\eta_Y}.$$

9. Show that the infinite plane wave results in Prob. 8 for the large- and small-scale fluctuations lead to the flux variance

$$\sigma^2_{I,\,\mathrm{pl}}(D_G) = \exp\left[\frac{0.49\sigma_R^2}{\left(1+0.65d^2+1.11\sigma_R^{12/5}\right)^{7/6}} + \frac{0.51\sigma_R^2(1+0.69\sigma_R^{12/5})^{-5/6}}{1+0.90d^2+0.62d^2\sigma_R^{12/5}}\right] - 1.$$

10. For an infinite plane wave, the spatial covariance function for weak irradiance fluctuations is defined by

$$B_{I,\,\mathrm{pl}}(\rho, L) = 16\pi^2k^2L\int_0^1\int_0^\infty \kappa\Phi_n(\kappa)J_0(\kappa\rho)\sin^2\left(\frac{L\kappa^2\xi}{2k}\right)d\kappa\, d\xi,$$

where $J_0(x)$ is a Bessel function. If we use the Gaussian function $K(x) = 8e^{-4x^2}$ to approximate the free-space MTF in Eq. (55) defined by

$$K(x) = \begin{cases} (16/\pi)\left[\cos^{-1} x - x\sqrt{1-x^2}\right], & 0 \le x \le 1, \\ 0, & x > 1, \end{cases}$$

(*a*) show that the resulting irradiance flux variance reduces to Eq. (59).
(*b*) Derive Eq. (60) from the result of part (*a*).

11. Based on Eq. (69) for the plane wave irradiance flux variance,
(*a*) deduce that under weak irradiance fluctuations

$$\sigma_I^2(D_G) \sim \frac{0.49\sigma_R^2}{(1+0.65d^2)^{7/6}} + \frac{0.51\sigma_R^2}{1+0.9d^2}, \qquad \sigma_R^2 \ll 1.$$

(*b*) From the result of part (*a*) for small apertures $d \ll 1$, show that

$$\sigma_I^2(D_G) \sim \left[1 - 0.83\left(\frac{kD_G^2}{4L}\right) + \cdots\right]\sigma_R^2, \quad \sigma_R^2 \ll 1, \quad \frac{kD_G^2}{4L} \ll 1.$$

(*c*) From the result of part (*a*), deduce that for large apertures $d \gg 1$ the irradiance flux variance can be approximated by

$$\sigma_I^2(D_G) \sim \left[0.81\left(\frac{kD_G^2}{4L}\right)^{-7/6} + 0.57\left(\frac{kD_G^2}{4L}\right)^{-1} + \cdots\right]\sigma_R^2,$$

$$\sigma_R^2 \ll 1, \quad \frac{kD_G^2}{4L} \gg 1.$$

12. Based on Eq. (77) for the spherical wave irradiance flux variance,
(*a*) deduce that under weak irradiance fluctuations

$$\sigma_I^2(D_G) \sim \frac{0.49\beta_0^2}{(1+0.18d^2)^{7/6}} + \frac{0.51\beta_0^2}{1+0.90d^2}, \qquad \beta_0^2 \ll 1.$$

(*b*) From the result of part (*a*) for small apertures $d \ll 1$, show that

$$\sigma_I^2(D_G) \sim \left[1 - 0.56\left(\frac{kD_G^2}{4L}\right) + \cdots\right]\beta_0^2, \qquad \beta_0^2 \ll 1, \qquad \frac{kD_G^2}{4L} \ll 1.$$

(*c*) From the result of part (*a*), deduce that for large apertures $d \gg 1$ the irradiance flux variance can be approximated by

$$\sigma_I^2(D_G) \sim \left[3.62\left(\frac{kD_G^2}{4L}\right)^{-7/6} + 0.57\left(\frac{kD_G^2}{4L}\right)^{-1} + \cdots\right]\beta_0^2,$$

$$\beta_0^2 \ll 1, \quad \frac{kD_G^2}{4L} \gg 1.$$

Section 10.4

13. Given Eqs. (114) and (115), show that

$$(a)\quad 0 < z < L_1\colon \gamma_1 = \frac{p(z)}{p(L)} = (\Theta - i\Lambda)\xi + (\Theta_2 - i\Lambda_2)(\Theta_3 - i\Lambda_3)(1-\xi),$$
$$\xi = 1 - z/L_1.$$

$$(b)\quad L_1 < z < L_2\colon \gamma_2 = \frac{p(z)}{p(L)} = (\Theta_2\Theta_3 - \Lambda_2\Lambda_3)(1+\xi) + (\Lambda_2\Theta_3 + \Theta_2\Lambda_3)\Omega_G\xi$$
$$+ i\Big[(\Theta_2\Theta_3 - \Lambda_2\Lambda_3)\Omega_G\xi - (\Lambda_2\Theta_3 + \Theta_2\Lambda_3)(1+\xi)\Big],$$
$$\xi = (L_1 - z)/L_2.$$

14. Given Eqs. (114) and (115), show that (see also Prob. 13)

$$(a)\ B_1(\xi) = L_2\left(1 - \frac{L_2}{F_G}\right) + L_3\left(1 - \frac{L_1}{F_G} - \frac{L_2}{F_g}\right)$$
$$+ L_1\left(1 - \frac{L_3}{F_g}\right)(1-\xi) + L_3\left(\frac{L_1L_2}{F_GF_g} - \Omega_G\Omega_g\right)(1-\xi)$$
$$+ i\Bigg[L_3\Omega_g + \left(1 = \frac{L_3}{L_2} - \frac{L_3}{F_G}\right)L_2\Omega_G(1-\xi)$$
$$+ \left(\frac{1}{L_2} - \frac{1}{F_G}\right)L_1L_3\Omega_G(1-\xi)\Bigg], \xi = 1 - z/L_1.$$

$$(b)\ B_2(\xi) = L_3 + L_2\left(1 - \frac{L_3}{F_g}\right)(1-\xi) + iL_3\Omega_g(1-\xi),\ \xi = (L_1 - z)/L_2.$$

References

1. H. T. Yura and S. G. Hanson, "Optical beam wave propagation through complex optical systems," *J. Opt. Soc. Am. A* **4**, 1931–1948 (1987).
2. H. T. Yura and S. G. Hanson, "Second-order statistics for wave propagation through complex optical systems," *J. Opt. Soc. Am. A* **6**, 564–575 (1989).
3. L. C. Andrews and W. B. Miller, "Single-pass and double-pass propagation through complex paraxial optical systems," *J. Opt Soc. Am. A* **12**, 137–150 (1995); "Single-pass and double-pass propagation through complex paraxial optical systems: Errata," *J. Opt Soc. Am. A* **12**, 2213 (1995).
4. A. E. Siegman, *Lasers* (University Science, Mill Valley, Calif., 1986).
5. J. W. Goodman, *Statistical Optics* (John Wiley, New York, 1985).
6. D. L. Fried, "Optical resolution through a randomly inhomogeneous medium," *J. Opt. Soc. Am.* **64**, 1372–1379 (1966).
7. A. H. Mikesell, A. A. Hoag, and J. S. Hall, "The scintillation of starlight," *J. Opt. Soc. Am.* **41**, 689–695 (1951).
8. V. I. Tatarskii, *Wave Propagation in a Turbulent Medium* (McGraw-Hill, New York, 1961), trans. by R. A. Silverman.
9. D. L. Fried, "Aperture averaging of scintillation," *J. Opt. Soc. Am.* **57**, 169–175 (1967).
10. A. I. Kon, "Averaging of spherical-wave fluctuations over a receiving aperture," *Radiophys. Quantum Electron*. **12**, 122–124 (1969).
11. R. F. Lutomirski and H. T. Yura, "Aperture-averaging factor of a fluctuating light signal," *J. Opt. Soc. Am.* **59**, 1247–1248 (1969).
12. J. H. Churnside, "Aperture averaging of optical scintillations in the turbulent atmosphere," *Appl. Opt*. **30**, 1982–1994 (1991).
13. L. C. Andrews, "Aperture-averaging factor for optical scintillations of plane and spherical waves in the atmosphere," *J. Opt. Soc. Am. A* **9**, 597–600 (1992).
14. E. L. Bass, B. D. Lackovic, and L. C. Andrews, "Aperture averaging of optical scintillations based on a spectrum with high wave number bump," *Opt. Eng*. **34**, 26–31 (1995).
15. L. C. Andrews, R. L. Phillips, and C. Y. Hopen, "Aperture averaging of optical scintillations: power fluctuations and the temporal spectrum," *Waves Random Media* **10**, 53–70 (2000).
16. L. C. Andrews, R. L. Phillips, and C. Y. Hopen, *Laser Beam Scintillation with Applications* (SPIE Press, Bellingham, Wash., 2001).